

ABSTRACT

Title of Dissertation: N-HETEROAROMATIC ACID ADLAYER STRUCTURES
UNDER HYDROGEN BONDING INFLUENCE:
A COMPREHENSIVE UHV-STM/XPS/RAIRS STUDY

Hui Li, Doctor of Philosophy, 2006

Dissertation directed by: Professor Janice E. Reutt-Robey
Department of Chemistry and Biochemistry

In this dissertation, I investigate the adsorption and growth of thin films of N-heteroaromatic acids and related molecules on Ag(111) surface. The N-heteroaromatic acids have ring-nitrogen and carboxylic groups. Hence, two primary hydrogen bond motifs are observed in their bulk crystal structures: head-to-tail hydrogen bond and tail-to-tail hydrogen bond. Furthermore, the high electron density of the aromatic rings increases the complexity of their electrostatic properties. The surface structure thus reflects the delicate balance between the intermolecular interactions and adsorbate-substrate interactions.

The surface adsorption model of isonicotinic acid (INA) is suggested based upon the STM and XPS study. The monolayer structure is stabilized by the head-to-tail hydrogen bonds along direction and weak side link hydrogen bonds. 12 rotational/reflection domains co-exist on the surface. Using reflection absorption infrared

spectroscopy (RAIRS), the layer-dependent orientation of the isonicotinic acid is determined. In the first monolayer, INA molecules exhibit 10° tilt angle to the metal surface. The second and third layers possess a combined twist ($\sim 20^\circ$) and tilt ($\sim 10^\circ$) orientation. This incline angle is contributed to the slight distortion (0.2%) along side link hydrogen bond direction upon the registration to the substrate.

With two additional aromatic rings, 9-acridine carboxylic acid (ACA) possesses a greater quadrupole. The surface structure is thus affected. The main interaction is still head-to-tail hydrogen bonding. However, electrostatic interactions are the main interactions to connect the head-to-tail chains. RAIR spectra reveal that at low coverage, the mobile species are head-to-tail linked. A proposed orientation of the monolayer films are given based upon the characteristic vibrational frequencies. The vibrational spectra of Anthroic acid (AA) are also done for the comparison reason. The orientation difference between the ACA monolayer and the AA monolayer are contribute to their electronic properties.

N-HETEROAROMATIC ACID ADLAYER STRUCTURES UNDER
HYDROGEN BONDING INFLUENCE:
A COMPREHENSIVE UHV-STM/XPS/RAIRS STUDY

By

Hui Li

Dissertation submitted to the Faculty of the Graduate School of the
University of Maryland, College Park in partial fulfillment
of the requirements for the degree of
Doctor of Philosophy,
2006

Advisory Committee:

Professor Janice E. Reutt-Robey, Chair
Professor Millard Alexander
Professor Theodore L. Einstein
Professor Amy Mullin
Professor Robert Walker

© Copyright by
Hui Li
2006

Table of Contents

List of Tables.....	iv
List of Figures	v
Glossary of abbreviations.....	viii
Chapter 1: Introduction	1
1.1 Self-assembly of Large Organic Molecules on Metal Surface: An Overview....	1
1.2 Background of Our Model System	4
1.3 Investigation Methods.....	8
1.4 Thesis Overview.....	8
Chapter 2: Experimental Setup	10
2.2 Description of the UHV Chambers	10
2.1.1 RAIRS UHV Chamber.....	10
2.1.2 XPS UHV Chamber	11
2.2 Substrate Preparation.....	14
2.3 Organic Thin Film Preparation	17
2.4 Data Acquisition and Analysis.....	18
2.4.1 Reflection-Absorption Infrared Spectroscopy	18
2.4.2 X-ray Photoelectron Spectroscopy.....	20
2.4.3 Scanning Tunneling Microscopy	20
Chapter 3: Hydrogen Bonded Sheets of INA on Ag(111).....	21
3.1 Introduction	21
3.2 Experimental Section	24
3.3 Results	25
3.3.1 STM Image.....	25
3.3.2 XPS Spectra.....	30
3.4 Discussion	32
3.5 Conclusions	35
Chapter 4: Layer Dependent Isonicotinic Acid Architecture on Ag(111).....	37
4.1 Introduction	37
4.2 Experimental Section	39
4.3 RAIRS Results	41
4.4 Discussion	46
4.5 Conclusions	58
Chapter 5: H-bond Directed Adlayer Architecture of Fused Aromatic Compounds: Contrasting AA vs. ACA on Ag(111).....	60
5.1 Introduction	60
5.2 Experimental Section	68
5.3 Results and Discussion.....	69
5.3.1 Theoretical Calculation	69
5.3.2 AA Adsorption on Ag(111) at 300 K.....	70
5.3.3 ACA adsorption on Ag(111) at 130 K.....	77
5.3.4 Temperature Dependent Measurements of ACA Monolayer	81

5.3.5 ACA Adsorption on Ag(111) at 300 K	83
5.4 Conclusions	86
Chapter 6: Thesis Conclusions	89
Appendix A Fabrication of Ta-Ta ₂ O ₅ Film	93
Appendix B Physical vapor deposition source	95
References	100

List of Tables

4.1	Scaled calculation results of INA monomer with assignments. The experimental results on cold and room temperature substrates are included.....	47
4.2	The experimental results compared with scaled calculated (UHF/6-31(d)) vibrational spectra of isonicotinic acid monomer, head-to-tail (H-T) dimer and tail-to-tail (T-T) dimer	48
5.1	Scaled calculation results of ACA monomer with assignments. The experimental results and condensed phase observations are included.....	71
5.2	Scaled calculation results of AA monomer with assignments. Experimental results and condensed phase observations are included.....	72

List of Figures

1.1	Ball-stick models of selected N-heteroaromatic carboxylic acids.....	5
1.2	Hydrogen bonding motifs of INA and ACA	6
2.1	Instrumental schematic of the RAIRS chamber.....	12
2.2	Kratos Axis 165 X-ray Photoelectron Spectrometer. (Reproduced from Kratos.com).....	13
2.3	Clean Ag(111) surface. STM images show (a) flat surface with large terrace area, (b) high step density region, and (c) step edge fluctuation at room temperature. LEED patterns demonstrate the C_6 symmetry of silver film.....	15
2.4	XPS survey spectrum of Ag(111) surface after a few cycles of sputtering/annealing. The lacking of peaks in O 1s and C 1s region indicates that the native contaminations are sufficiently removed.....	16
2.5	RAIR spectra of ACA on Ag(111) surface. A flat 100% baseline is included.....	19
3.1	Schematic drawing of (a) isonicotinic acid molecule, (b) head-to-tail hydrogen bonded arrangement, (c) tail-to-tail hydrogen bonded arrangement, and (d) crystal structure of isonicotinic acid.....	23
3.2	A CCT-STM image of 0.7 ML INA on Ag(111). INA domains typically exist in rhombic shapes due to the anisotropic intermolecular interactions: the sharp boundary is along the primary H-bond direction which is along the $Ag[1\bar{1}2]$, while the noisy boundary is along the secondary H-bond direction.....	26
3.3	STM images (a and b) and proposed structural models (c and d) of two INA ordered structures which demonstrate mirror symmetry with respect to the $Ag[1\bar{1}2]$ direction. For reference, a unit cell is indicated in each panel, along with the matrix notation of the domain. Ag(111) lattice vectors are shown in (c). Constant-current ($50 pA$) STM images ($8 \times 8 nm^2$) were acquired with a $-0.8 V$ negative sample bias.....	28

3.4	(a) An STM image demonstrating the coexistence of different INA domains on Ag(111). A and B are rotated by 180° relative to each other. (b) and (c) Magnified STM images of the boxed areas I and II in (a), superimposed with the suggested INA molecular packing models.....	29
3.5	N 1s and O 1s X-ray photoemission spectra of 0.7 ML INA on Ag(111) surface (open circles) with linear least-squares fit to Gaussian functions (line). The binding energies of the fitting components are marked in the figure.....	31
4.1	RAIR spectra of isonicotinic acid adsorbed on Ag(111) at room temperature. The coverage is (from top to bottom): 0.25ML, 0.6ML, 1ML and multilayer. IR spectrum of INA bulk crystal is also included at the bottom.....	42
4.2	RAIRS spectra of isonicotinic acid adsorbed on Ag(111) at 135 K. The coverage is (from top to bottom): 0.1ML, 0.2ML, 0.6ML and 1.0 ML. An IR spectrum of INA bulk crystal is included at the bottom.....	43
4.3	RAIR spectra of 1 monolayer of INA adsorbed on Ag(111).....	44
4.4	schematic drawing of (a) side-view of out-of-plane C-H mode (861 cm^{-1}); (b) side-view of $-\text{C}=\text{C}-$ in phase scissoring mode (1412 cm^{-1}); (c) top-view of 861 cm^{-1} mode; (d) top-view of 1412 cm^{-1} mode. The transition dipole moments are illustrated as bold arrows.....	52
4.5	The ratio of integrated IR absorption intensity of 1412 cm^{-1} band to 858 cm^{-1} band versus the isonicotinic acid coverage adsorbed on Ag(111) at room temperature.....	54
4.6	Suggested model of layer-by-layer INA adsorbed structures on Ag(111).....	57
5.1	Schematic drawings of (a) ACA molecule. A dihedral angle of 78.9° is illustrated, (b) hydrogen bond arrangements, and (c) bulk crystal structure of ACA hydrate. ACA molecules are bonded by head-to-tail couplings with a twisted orientation.....	61
5.2	Schematic drawings of (a) AA molecule. A dihedral angle of 54° is illustrated, (b) hydrogen bond arrangement, and (c) bulk crystal structure of AA. AA molecules are bonded by tail-to-tail couplings with a twisted orientation.....	63

5.3	STM images and schematic model of ACA adsorption on Ag(111) at room temperature. (a) co-existing of chain phase (A) and dimer phase (B). Molecular resolved images of (c) chain phase and (d) dimer phase are shown. A schematic compositional phase diagram is included in (b). (reproduced from JACS, 2006 , <i>128</i> , 8493)	64
5.4	The proposed structure model of (a) chain phase and (b) dimer phase, respectively. Unit cells are pointed out. Each unit cell of the chain phase contains two inequivalent ACA molecules. There are four molecules in each unit cell of the dimer phase. (reproduced from JACS, 2006 , <i>128</i> , 8493).....	65
5.5	STM images of AA adlayer structures on Ag(111) at room temperature: (a) 200 nm X 200 nm image reveals coexistence of AA phases I (2-D gas), II (1 st dimer phase), III (2 nd dimer phase) and IV (bilayer phase), (b) magnified image of 2 nd dimer phase and AA bilayer, (c) magnified image of 1 st dimer phase, showing resolution of AA dimers.....	67
5.6	RAIR spectra of AA assembly on Ag(111) at room temperature.....	74
5.7	Schematic illustration of C-H out-of-plane bending and C=C stretch modes. The transition dipole moments are illustrated as bold arrows.....	76
5.8	A set of coverage dependent RAIR spectra of ACA adsorption on Ag(111) at 135K. The bottom trace is a reference spectrum of ACA in condensed phase.....	78
5.9	A set of temperature dependent RAIR spectra of 1 ML of ACA films on Ag(111). From top to bottom, the corresponding temperatures are: 135 K, 200 K and 300 K.....	82
5.10	A set of coverage dependent RAIR spectra of ACA adsorption on Ag(111) at room temperature. The bottom trace is a reference spectrum of ACA in condensed phase.....	84
5.11	Schematic illustrations of ACA chain structure, based upon fixed 78° dihedral angle. Model depicts two inequivalent ACA per unit cell, as observed in STM images, in tilt and twist orientation. Tilt and twist angle of ~ 50° and 45°, respectively.....	87

Glossary of Abbreviations

AA	9-anthroic acid
ACA	9-acridine carboxylic acid
INA	Isonicotinic acid
NHA	N-heteroaromatic acid
DOS	Density of states
FTIR	Fourier transform infrared
HREELS	High resolution electron energy loss spectroscopy
NEXAFS	Near-edge X-ray absorption fine structure
RAIRS	Reflection-absorption infrared spectroscopy
SAM	Self-assembled monolayer
STM	Scanning tunneling microscope
TPD	Temperature programmed desorption
UHV	Ultra high vacuum
UPS	Ultraviolet photoelectron spectroscopy
XPS	X-ray photoelectron spectroscopy

Chapter 1

Introduction

1.1 Self-assembly of Large Organic Molecules on Metal Surfaces: An Overview

The adsorption of large organic molecules on metal surfaces has attracted intensive attention recently because it provides a promising route to generate functional systems within the nanoscale. Current fabrication methods of the microelectronics industry are approaching their fundamental limits¹. The emergence of nanotechnology has ignited a “bottom-up” approach to fabricate microelectronic devices. Instead of classic manufacturing, self-assembly of organic films on metal surfaces provides a convenient strategy to create surface nanostructures, which are suitable for applications involving molecular electronic² and optoelectronic devices.³ Molecular self-assembly is the spontaneous association of molecules into stable, structurally well-defined aggregates joined by specific noncovalent interactions, such as hydrogen bonding⁴⁻⁸, dipole-dipole coupling^{9, 10} and metal-ligand interaction.^{11, 12} In general, superstructures on metal surfaces are controlled by the delicate balance of intermolecular forces and molecule-surface interactions. Surface structures even can be tuned by varying the substrate’s physical or chemical properties, such as temperature and impurity concentration. Fundamental understanding of the structure and organization of thin molecular films is therefore valuable.

Self-assembled monolayer (SAM) formation can be traced back to 1946, when Zisman published the preparation of a monomolecular layer by adsorption of a

surfactant onto a clean metal surface. At that time, the importance of self-assembly was not fully recognized. More recently, interest in SAMs was provoked by Nuzzo and Allara in 1983.¹³ They found that SAMs of alkanethiolates on gold could be prepared by adsorption of di-n-alkyl disulfides from dilute solutions. The layer-by-layer self-assemblies prepared in solution have been investigated intensively over the last two decades. Typical organic molecules studied include thiols¹⁴⁻¹⁶ and fatty acids.¹⁷⁻²⁰ The common feature is adsorbates form strong chemical bonds to the substrate through a surface-active head group, with the intermolecular interactions between the tail groups driving the formation of closely-packed and ordered SAMs. Solution based deposition is easy to set up, and forms dense functionalized surfaces. However, there are some shortcomings of this technique. First, the surfaces must be inert toward corrosion or oxidation; consequently most of the studies involve gold surfaces. Secondly, SAMs strongly chemisorb on the surface, and the spontaneously formed structures are hard to manipulate. To achieve the goal of manipulating the surface structures, thorough studies of weakly bounded supramolecular films are essential.

Aromatic carboxylic acids adsorbed on metal surfaces are hence attractive. Aromatic carboxylic acids are significant because they can form either strong or weak chemical bonds to metal surfaces. On active transition metal surfaces, carboxylic acids can undergo complex reactions. It is known that adsorption of benzoic acids onto Cu(110)²¹ and Ni(110)²² leads to the room temperature deprotonation of the acid group into the carboxylate functionality at room temperature, forming strong chemical bonds through carboxylate oxygen to the substrate. Consequently,

perpendicular orientations are observed. On the other hand, aromatic systems weakly chemisorb on noble metal surfaces through π bonding and present parallel orientations.²³ Thus, the adsorption and growth of aromatic carboxylic acids on different substrates provides insight on the impact of competitive adsorbate-substrate interactions.

Recently, many studies have been directed toward aromatic carboxylic acids^{6, 24-28}, which exhibit flat-lying geometries upon surface adsorption. By choosing the appropriate substrate material and symmetry, the sensitive balance of intermolecular and molecule-substrate interactions can be tuned to obtain well-defined supramolecular architectures. Compared to the SAMs formed via solution-based methods, the chemisorption bonds formed by interactions between the aromatic rings and the metal surfaces, are weak. Surface adlayers can be easily contaminated. Therefore, the carboxylic acid films are prepared by physical vapor deposition in ultrahigh vacuum. This technique has a few practical advantages: It is carried out in ultrahigh vacuum that is a super clean environment. It enables precise control of substrate temperature, growth rate, and film thickness. It provides the possibility to perform complementary *in situ* characterizations with many vacuum techniques.

The key intermolecular interactions to stabilize aromatic carboxylic acid surface structures are hydrogen bonding and π - π interactions. Hydrogen bond linked supermolecules are found with widely varying surface arrangements that include 1-D chains²⁴, 2-D sheets^{24, 26} and extended networks.²⁹ Primary hydrogen bonds include OH \cdots O, OH \cdots N bonds with bonding energies in the range of 10 ~ 15 kcal/mol. Secondary hydrogen bonds are also found in aromatic carboxylic acid systems. Ring

attached hydrogen can serve as proton donors, forming weak CH...O hydrogen bonds (~ 2 kcal/mol); Hydrogen bond donors can also interact with the high electron density of the aromatic π cloud (1 to 2 kcal/mol).³⁰

1.2 Background of our Model System

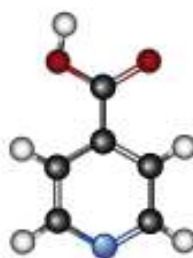
This thesis will focus on the adsorption of molecules from the N-heteroaromatic carboxylic acid (NHA) family on Ag(111). Representative NHA molecules are pictured in Figure 1.1. Nicotinic acid is one type of vitamin B (commonly called niacin); isonicotinic acid (INA) is broadly used in treating tuberculosis³¹ and used as matrix material in bio-analytical chemistry; and 9-acridine carboxylic acid (ACA), especially its complexes, attract intensive interest in medical research.³²

Besides the biological importance of these NHA compounds, NHAs are fundamentally interesting for their anisotropic intermolecular interactions. Each NHA molecule presents one hydrogen bond donor (hydroxyl group) and two hydrogen bond acceptors (carbonyl group and ring nitrogen). Hence, NHA molecules can form two types of primary hydrogen bonds: either from the ring nitrogen to the neighboring molecule's carbonyl oxygen (head-to-tail H-bond) or between two molecules' carboxylic groups (tail-to-tail H-bond) (see Fig. 1.2). In both niacin and INA bulk crystals, molecules display chain-like head-to-tail H-bond arrangements in each layer and π - π interactions between the layers.³³ X-ray diffraction investigations of ACA dihydride crystals reveal that head-to-tail hydrogen bonding is also the dominant interaction between these polycyclic molecules. However, since ACA has a

nicotinic acid



isonicotinic acid



- carbon
- oxygen
- nitrogen
- hydrogen

9-acridine carboxylic acid



Fig 1.1 Ball-stick models of selected N-heteroaromatic carboxylic acids.

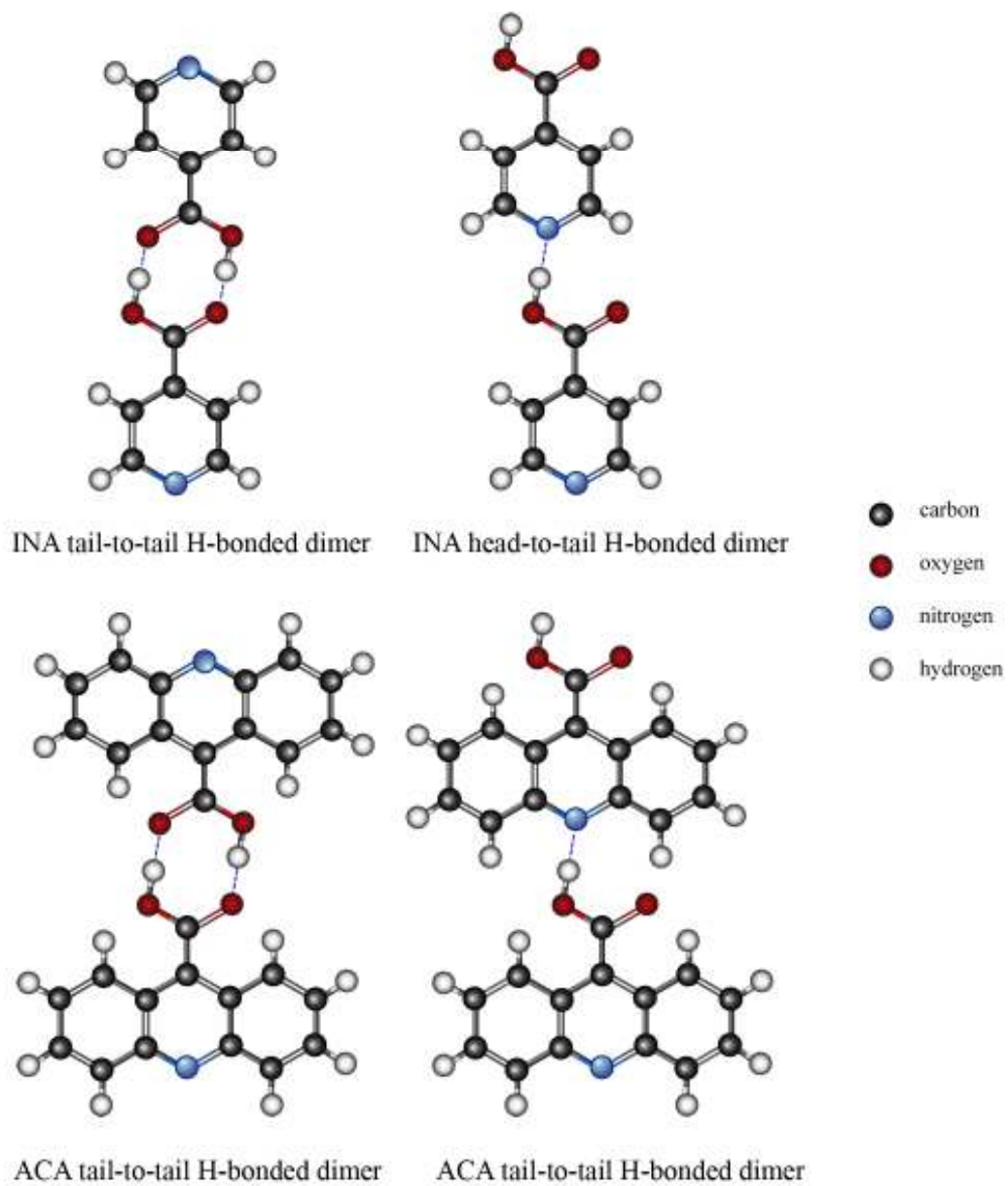


Fig. 1.2 Hydrogen bonding motifs of INA and ACA, shown schematically

greater quadrupole and greater electron density than both niacin and INA, the dispersive and electrostatic interactions between molecules push a zigzag orientation in each layer.

Surface science studies of these intriguing molecules are limited to date. O'Shea and colleagues studied INA adsorption on TiO₂ by STM, XPS and XAS.^{34, 35} INA deprotonates on TiO₂ and presents a perpendicular orientation at room temperature. Angle dependent XPS studies reveal that INA molecules in multilayer films form head-to-tail hydrogen bonds, similar to the bulk crystal. However, INA adsorption on noble metal surfaces remains unexplored. The surface chemistry of other NHAs remains largely unexplored. Reported ACA studies have utilized STM and XPS to deduce 2-D film structures.^{36, 37}

In this dissertation, I studied NHA adsorption on Ag(111) films. Silver low index surfaces have been investigated intensively; thus, their properties are well understood. Moderate activities are observed on these surfaces. Early on, Demuth *et al.* investigated small aromatic molecules (benzene, pyridine and pyrazine) on Ag(111).²³ Parallel adsorption geometries through π bonding were deduced for benzene and pyrazine. Pyridine showed a transition from flat lying geometry at low coverages (< 0.5 L), rearranging to an inclined geometry at high coverages. Binding energies of 10 to 12 kcal/mol indicated that these molecules weakly chemisorbed on the surface. Meanwhile, Parker and his colleagues demonstrated that monocarboxylic acids deprotonate on pre-oxidized Ag(111) and Ag(110) at room temperature, but remain intact on the neat Ag(111).³⁸ Consequently, Ag(111) provides an ideal basis to study NHAs adsorption.

1.3 Investigation Methods

To address the architectures of the surface adlayers, I have investigated NHA adsorption on Ag(111) with two probes: RAIRS and XPS. These spectroscopic investigations provide information that is completely complementary to the STM investigations performed in parallel in our group. STM provides information on the morphology of the surface on length scales ranging from atomic to mesoscopic dimensions, on the 2-D spatial arrangements of the adsorbates and the lattice constants of the supramolecular structures. But the interpretation of STM images in terms of real space models is problematic. Instead of molecular architecture, STM senses electronic density of states (DOS) near the Fermi level most directly. The DOS does not equate the molecular structure especially for semiconductor molecules, which are 3-D in nature. In contrast, spectroscopy is more of a local probe of structure. RAIRS and XPS determine both the chemical identity and the surface orientation of adsorbed species. The combination of these techniques provides unambiguous means to reveal the properties of the surface architectures.

1.4 Thesis Overview

This thesis will present a detailed characterization of the formation and growth of self-assembled supramolecular structures. The main body of this thesis divides into four chapters. Chapter 2 describes the experimental methods, including the ultra high vacuum systems, silver film preparation and organic film deposition. XPS, RAIRS and STM measurements and data analyses are also covered in this chapter.

Chapter 3 presents the 2-D network formed upon the adsorption of isonicotinic acid on Ag(111). The size of the unit cell of INA films suggests a molecular adsorption and the molecules adsorbed on surface with a near parallel orientation. N 1s core level shift indicates that head-to-tail hydrogen bonds are the dominant interactions to stabilize the surface aggregates. A 2-D model is given based on the XPS and STM data. INA films are described as molecular sheets with head-to-tail couplings along the $[1\bar{1}0]$ direction, and the weak side-link hydrogen bonds connect the head-to-tail chains into 2-D films.

Chapter 4 focuses on RAIRS investigations on INA adlayer structures. Surface vibrational spectra confirm the essential features of 2-D structures proposed in Chapter 3. Further analyses reveal that the first monolayer of INA molecules adsorbs on Ag(111) in a near-parallel orientation with a tilt angle of $\sim 10^\circ$. This tilt angle is shown to increase for multilayer films. A combination of tilt and twist orientation is proposed for both second and third layers.

Chapter 5 focuses on the thermal aggregation of 9-acridine carboxylic acid (ACA) on Ag(111). Temperature dependent RAIRS spectra reveal the films transition from kinetically controlled growth to thermodynamically controlled growth as the substrate temperature is raised from 135 K to 300 K. Comparative vibrational studies with 9-anthracic acid (AA), are used to decipher H-bonding motifs. At reduced temperatures we deduce a head-to-tail H-bonding motif with different ACA chain lengths.

Chapter 2

Experimental Procedures

Organic molecular adsorption on metal surfaces has both fundamental importance and practical potential. Recently, numerous studies have focused on the structure and growth of ultrathin molecular films. Experimental techniques applied to molecular films include STM^{4, 6, 39, 40}, XPS^{41, 42}, UPS⁴³, NEXAFS⁴², TPD⁴⁴, HREELS^{42, 45, 46}, and RAIRS.^{44, 47, 48}

In this study, three UHV techniques are used to characterize organic films adsorbed on Ag(111): XPS, STM and RAIRS. Experiments were conducted in three separate ultrahigh vacuum (UHV) systems, each with base pressures of 1.0×10^{-10} torr or better. The general principles of these surface science techniques can be found in many texts.^{49, 50} This chapter provides specific information on the experimental systems and methods for the data acquisition and analysis, used in this dissertation.

2.1. Description of the UHV Chambers

2.1.1 RAIRS UHV Chamber

Reflection absorption infrared spectroscopy was performed in a homemade two-level ultra-high-vacuum chamber.⁵¹ The schematic diagram of the UHV chamber is shown in Fig. 2.1. The bottom level is connected to the load lock for easy sample transfer and exchange. Auger electron spectroscopy is equipped in the same level. The upper level is equipped with mass spectrometer for checking the residual gas, ion gun for sample cleaning, and a commercial deposition source (SPECS

NATC) for physical vapor deposition. A FTIR spectrometer is optically coupled to the UHV chamber at the same level. During deposition and data acquisition, the metal substrate is suspended from a commercial UHV manipulator (McAllister Technical Services) that is capable of XYZ translation and a 360° polar rotation. A cooling Dewar is integrated to the manipulator via a 2-3/4 flange. The sample mount assembly is suspended from a copper block at the base of the Dewar and is electrically isolated by sapphire washers. With this configuration, the sample can be cooled down to 135 K with liquid nitrogen. The heating assembly is mounted on the back of the sample mount, consists of a 0.010-inch diameter spiral tungsten filament. The sample can also be heated by direct electron bombardment. During electron bombardment, the sample is positively biased at up to 1 KV. In the absence of liquid nitrogen, 25 mA thermionic emission and a sample bias of 600 V is needed to heat the silver sample to 800 K.

2.1.2 XPS UHV Chamber

The X-ray photoelectron spectroscopy was performed in a commercial UHV system (Fig. 2.2). A gate valve separates the system into two chambers: an analyses chamber and a preparation chamber. In the preparation chamber, a home-built Knudsen cell is mounted for organic molecule deposition and a load-lock for sample transferring. The analyses chamber is equipped with Kratos AXIS 165 spectrometer for data acquisition, a differentially pumped sputter gun for surface treatment and a commercial UHV manipulator for XYZ translation and polar rotation of the

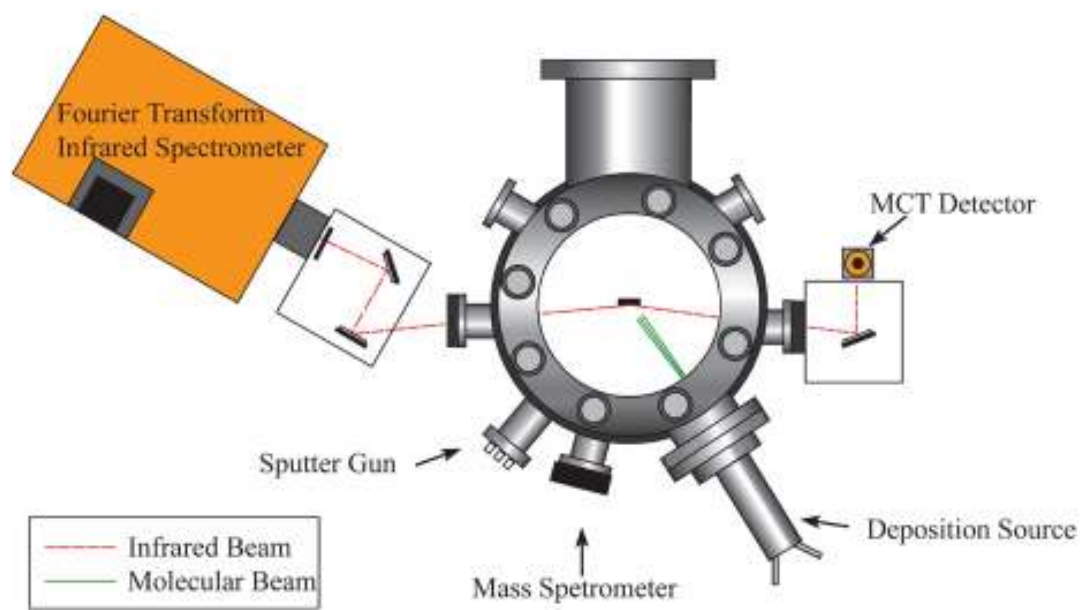


Fig 2.1. Top view schematic of the RAIRS chamber



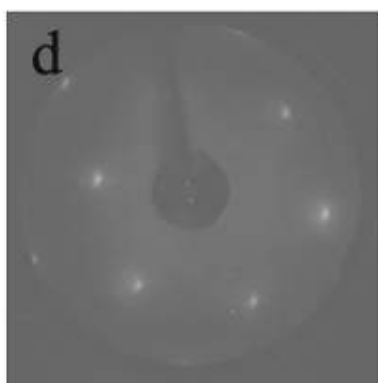
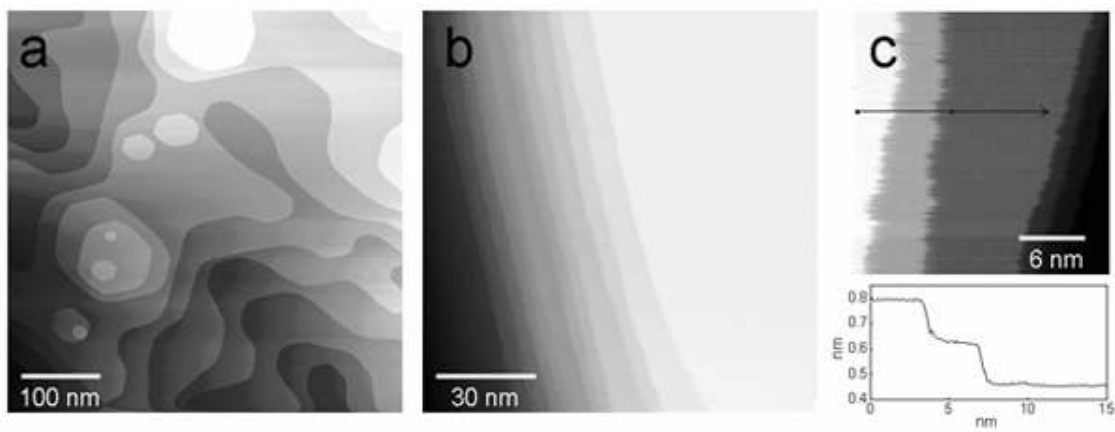
Fig. 2.2 Kratos Axis 165 X-ray Photoelectron Spectrometer. (reproduced from Kratos.com)

substrates. The sample stage mounted on the manipulator can be cooled down to 170 K and heated up to 750 K.

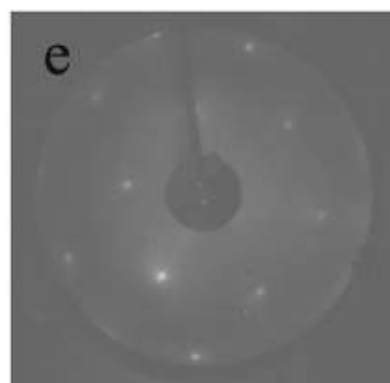
2.2. Substrate Preparation

The substrates we use in the experiments are Ag(111) films supported on mica discs. Ag(111) films are prepared by physical vapor deposit silver onto freshly exfoliated mica discs.⁵² The mica discs are pressed against a tungsten ribbon of comparable size and heated by direct current through the ribbon to a temperature of 700 K. Before deposition, the mica discs are degassed at 600K for one hour in a chamber with base pressure less than 1×10^{-6} torr. During the deposition, the mica discs are held at 700K. The deposition rate is guided by a quartz microbalance (INFICON XTM/2). A deposition rate of 80 angstrom per second is preferred to achieve an atomically flat surface. The initially prepared Ag films (*ca.* 500 nm thickness) are transferred through air into separate UHV chambers for STM, XPS and RAIRS investigations.

The Ag(111) films are then cleaned with a series of sputter-anneal cycles under UHV conditions. Before sputter-anneal cycles, the sputter position was calibrated by Ta₂O₅ film. (See Appendix I) Argon ion sputtering was performed on room temperature films and the sputtering condition is 1000V, 50 μ A. Subsequent annealing to 800K for 20 minutes efficiently remove most sputtering damages. The substrates' structure and impurities were checked by multiple techniques. We found that after three to five sputter-anneal cycles, a surface with negligible surface impurities can be obtained (see Fig. 2.3). At this stage, native oxygen and surface



Electron energy: 148.3 eV



Electron energy: 199.4 eV

Fig. 2.3 Clean Ag(111) surface. STM images show (a) flat surface with large terrace area, (b) high step density region, and (c) step edge fluctuation at room temperature. LEED patterns demonstrate the C₆ symmetry of silver film.

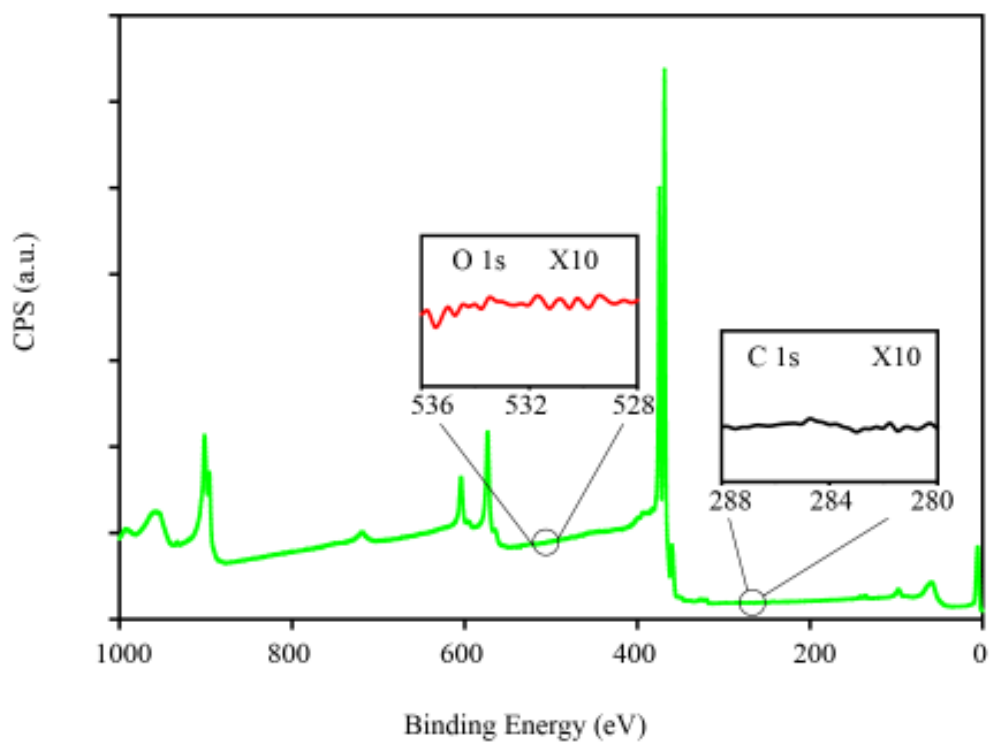


Fig 2.4. XPS survey spectrum of Ag(111) surface after a few cycles of sputtering/annealing. The lacking of peaks in O 1s and C 1s region indicates that the native contaminations are sufficiently removed.

carbon were below the detect limit of XPS. Fig. 2.4 shows a XPS spectrum of the clean Ag(111) surface.

2.3. Organic Thin Film Preparation

In this dissertation, three molecular sources, isonicotinic acid (INA), acridine carboxylic acid (ACA) and anthroic acid (AA) are studied. All three molecules are commercially available. INA (99.8%, Aldrich) is a white powder, and both ACA (98%, Aldrich) and AA(99%, Aldrich) are yellow powders.

For STM and XPS experiments, the organic thin films were prepared in the sample transferring chambers. The organic powders were placed in home-made quartz Knudsen cells and degassed for at least 4 hours (65° C for INA, 80° C for both ACA and AA) to remove more volatile impurities. The cell temperature was then raised to the deposition temperature. During deposition, room temperature substrates were positioned 5 cm away from the Knudsen cell.

For RAIRS experiments, the transition and vibration of the sample will cause unstable baseline. Therefore, the thin films were made *in situ*. A commercial low temperature Knudsen Cell (SPECS NATC) was mounted in front of the sample position. The cell was positioned 30 cm from the sample, placing the shutter 2.54 cm away from the substrate. The chemicals were degassed as described previously. Molecular deposition was performed as a function of substrate temperature. The following RAIRS measurements were taken at corresponding adsorption temperature.

2. 4. Data Acquisition and Analysis

2.4.1 Reflection-Absorption Infrared Spectroscopy

Infrared vibrational measurements were conducted on a Nicolet Nexus 670 FTIR spectrometer optically coupled to the UHV chamber. The p-polarized IR radiation from a broad band IR source was reflected from a flat mirror and focused by an f/12 paraboloidal mirror to the sample at grazing angle ($\theta = 85^\circ$) through a differentially pumped KBr window. The reflected beam exited the chamber through another differentially pumped KBr window, recollected by an ellipsoidal mirror and detected by a liquid nitrogen cooled mercury cadmium telluride (H*-MCT) detector with a spectral range of 800-4000 cm^{-1} . The non-UHV optical path is enclosed in plexiglass and purged by air that is dried and scrubbed of $\text{CO}_2(\text{g})$.

The spectra were collected in the form of double-sided interferograms at 4 cm^{-1} resolution. Interferograms were zero-filled and apodized by triangular apodization. Before each deposition, a few background spectra were collected until a flat baseline can be obtained (see Fig. 2.5). The vibrational spectra were then obtained by taking the ratio of the sample reflectivities to the stable clean background. Typical spectra were collected with 1024 scans except mentioned otherwise. The spectra are saved as JDX files, which can be converted into data pairs. The data pairs are then inputted into Sigma Plot for further analyzing and plotting.

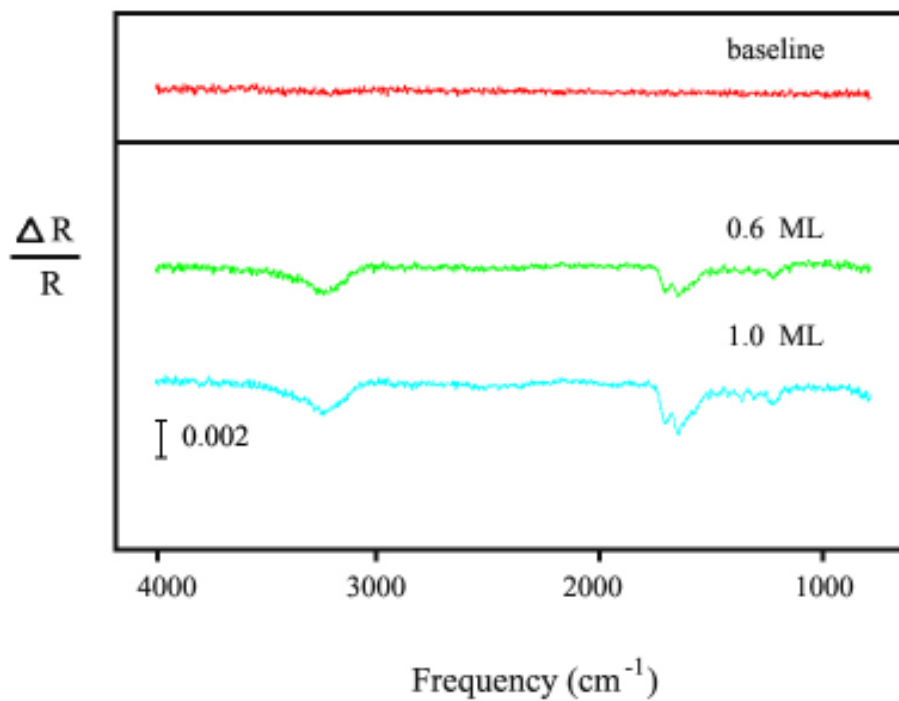


Fig. 2.5 A set of RATR spectra showing (a) 100% flat baseline obtained as ratio of clean Ag(111) to clean Ag(111) and (b) ACA on Ag(111) at 135 K, referenced to the clean Ag(111) surface.

2.4.2. X-ray Photoelectron Spectroscopy

XPS experiments were performed with Kratos AXIS 165 spectrometer with a base pressure of 3×10^{-10} torr using the Mg K α excitation line (1253.6 eV) at room temperature. Co-addition of 40 scans is chosen to avoid radiation damage of the organic films.

The XPS data are acquired as Kratos datasets, which can be converted into a standard VMS format. The VMS files are then exported to CasaXPS where they can be further processed. The output is finally plotted using Sigma Plot.

2.4.3. Scanning Tunneling Microscopy

STM experiments were conducted with a room temperature STM (Omicron STU-52) and an Omicron VT-STM with a base pressure of 1×10^{-10} torr or better. The probe tips were electrochemically etched tungsten wires (0.25 mm in diameter, 99.95%). The tips were subsequently cleaned under UHV by electron bombardment (200 V, 10 μ A) prior to data acquisition to remove the oxide and contaminants. Details of the probed tip preparation can be found in previous work. The reported images were collected in a constant current mode with a typical sample bias of +0.8 V and a typical tunneling current of 50 pA. These relatively mild tunneling conditions were chosen to minimize the tip-sample interaction. The data were processed using IDL (Interactive Data Language). The piezoelectric scanner was calibrated with atomically resolved images of the Ag(111) surface. Based upon the unit cell constants of Ag(111), the raw data were scaled by 0.95 along the X direction and 1.1 along the Y direction.

Chapter 3

Hydrogen Bonded Sheets of INA on Ag(111)

3.1. Introduction

Self-assembled nanoscale structures, stabilized by non-covalent interactions such as hydrogen bonding⁴⁻⁶, metal-ligand interaction¹² and dipole-dipole interaction¹¹, are under extensive investigation. Detailed knowledge of assembly principles will provide invaluable insight for nanofabrication, eventually leading to nanostructures that build themselves directly into microelectronic devices¹⁰.

Knowledge of solid-state molecular systems (especially crystals) provides an important reference for molecular nanofabrication. Molecular orientation and packing in the solid state are dominated by intermolecular interactions. Surface nanostructures are assembled by the same interactions, with the added influence of the substrate and reduction in dimensionality. Exploring the relationship between bulk crystal structure and surface architectures thus reveals the impact of substrate and dimensionality on molecular nanostructures^{9, 27, 53}.

In this chapter, I examine the relationship between surface and bulk molecular architecture for the case of isonicotinic acid (INA). Based upon its pronounced orientation-dependent interactions, INA is a useful model system for studying self-assembly. Several previous self-assembled studies have focused on carboxylic acid molecules on metal surface^{6, 26, 54-56}. Carboxylic acids provide hydrogen bonds with selectivity and directionality that determine the size and shape of surface nanostructures. In the case of isonicotinic acid, the presence of a ring nitrogen atom,

introduces additional chemical functionality that is at the core of isonicotinic acid's biological activity^{57, 58} and allows INA to function as a molecular tether in organic photocells⁵⁹. The assembly patterns of this molecule are thus of both fundamental and practical interest.

Isonicotinic possesses two hydrogen bonding motifs: from ring nitrogen to hydroxyl group (head-to-tail h-bond) or between the carboxyl groups (tail-to-tail h-bond), as shown in Figure 3.1. First principles calculations indicate that the tail-tail linkage, which involves two hydrogen bonds, is energetically preferred to the head-to-tail linkage, which involves one hydrogen bond⁶⁰. However, the strength of the head-to-tail linkage *per hydrogen bond* exceeds that of the tail-to-tail linkage *per hydrogen bond*. Consequently, tail-to-tail geometries are favored by dimers, but extended assemblies of INA molecules should favor head-to-tail arrangements. The bulk structure of INA adopts such a head-to-tail arrangement, in which INA molecules are linked by means of O-H \cdots N hydrogen bonds along the *b* axis into chains. These chains are joined by secondary hydrogen bonds between aromatic hydrogen and carbonyl oxygen to form a molecular sheet parallel to the (100) plane. Within this molecular sheet, all INA chains run in the same direction, but the direction alternates between neighboring sheets, as shown in Figure 3.1³³.

In our experiments we use scanning tunneling microscopy (STM) and complementary X-ray photoelectron spectroscopy (XPS) to determine the molecular architecture of monolayer films of INA on Ag(111). STM images were collected mainly by Bo Xu. Through a direct comparison of the monolayer and bulk molecular architectures, we deduce the key interactions that govern robust film architecture. In

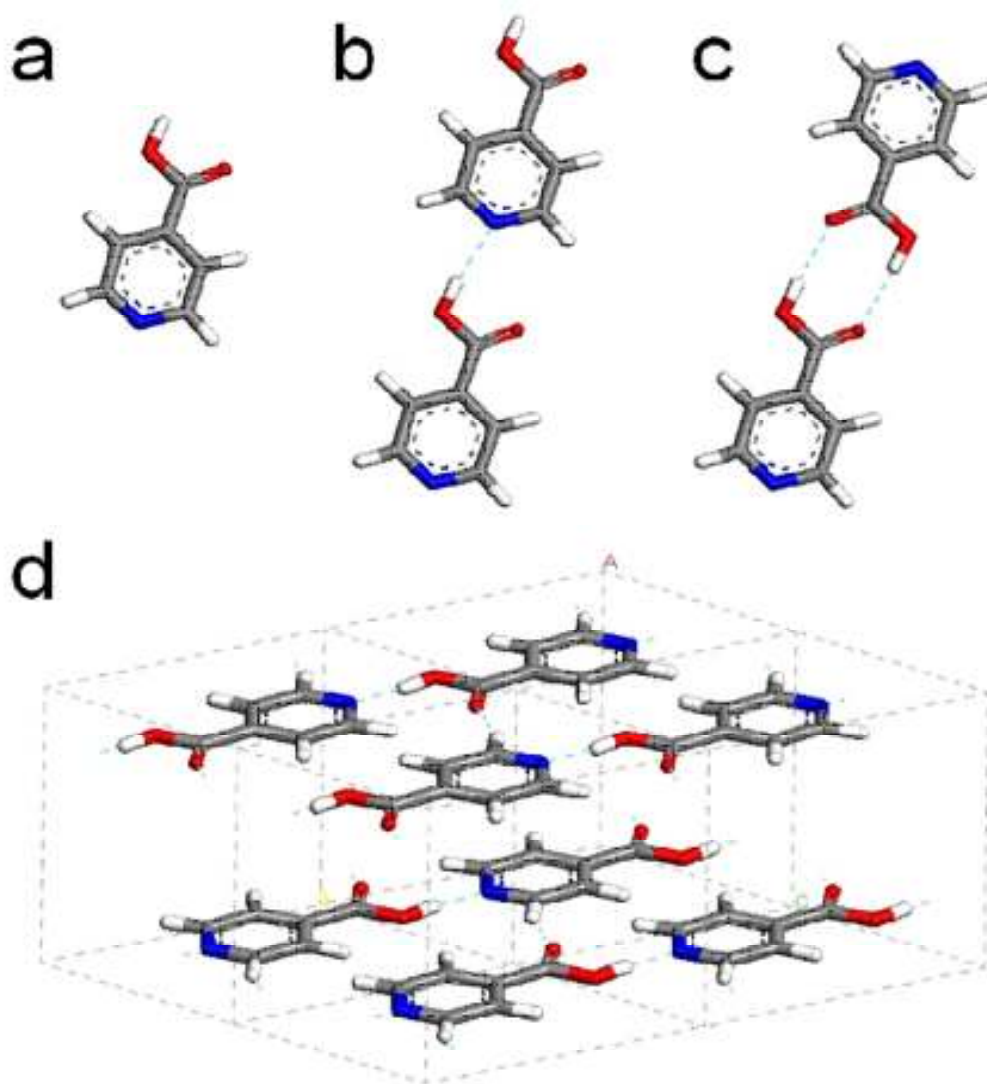


Fig. 3.1 Schematic drawing of (a) isonicotinic acid molecules, (b) head-to-tail hydrogen bonded arrangement, (c) tail-to-tail hydrogen bonded arrangement, and (d) crystal structure of isonicotinic acid.

particular, we show that the bulk head-to-tail H-bonding motif extends toward the monolayer architectures with minimal adaptation to the Ag(111) support. This distinctive adlayer architecture gives rise to distinctive orientational domains. We describe how film microstructure and stability are set by the H-bonding interactions along the boundaries of these orientational domains.

3.2 Experimental Section

Experimental measurements were conducted in two separate ultrahigh vacuum chambers. STM experiments were performed with an Omicron UHV STM system at room temperature in a system with a base pressure less than 1×10^{-10} torr. All reported images were collected in a constant current mode. Relatively mild tunneling conditions were chosen in this study to minimize the interaction between the tip and the molecules. XPS experiments were performed with a Kratos AXIS 165 spectrometer with Mg K_{α} excitation line (1253.6 eV) in a separate system. The base pressure is in the low 10^{-10} torr. All experiments are performed at room temperature. All XPS spectra are calibrated by Ag $3d_{5/2}$ core level spectrum.

The substrates used in these studies are 500 nm thick Ag(111) films, which are prepared by physical vapor deposition on mica supports⁵². The films are processed by cycles of Argon ion sputter (1000 V, 0.5 μ A) and subsequent annealing to 800 K, leading to atomically smooth Ag(111) films with typical terrace widths over 100 nm³⁶. The INA powder (Aldrich, >99%) was loaded into a home-built Knudsen Cell evaporator (quartz crucible) and outgassed at 60 °C under vacuum for several hours. All depositions were performed in the vacuum loadlocks of the two respective

ultrahigh vacuum chambers, where the base pressure is $< 1 \times 10^{-8}$ torr. The INA was sublimed at a temperature of 85°C onto room temperature Ag(111) substrates. This provides a deposition rate of about one monolayer per 5 minutes. Here we define one monolayer of INA coverage as one INA molecule per six surface Ag atoms. Immediately after INA deposition, the films were directly transferred to the UHV chambers for STM and XPS measurements.

3.3 Results

3.3.1. STM Image

STM images show the evolution of INA molecular films with increasing coverage. Monolayer films grow via the formation and subsequent coalescence of INA molecular islands. An STM image of 0.7 ML INA on Ag(111) is shown in Figure 3.2. The INA islands are imaged as dark regions and exhibit characteristic rhombic shapes. Island boundaries (away from Ag crystallographic steps) are remarkably straight, particularly those edges that are aligned along the substrate $[11\bar{2}]$ direction.

The mosaic structure in Figure 3.2 indicates the coexistence of different INA domains on the Ag(111) surface. Molecularly resolved STM images show that all domains possess the same molecular architecture. Figure 3.3 provides STM images of two distinct enantiomeric domains. Individual molecules appear as protrusions, forming a hexagonal superstructure commensurate with the Ag(111) substrate. The unit cells for these two INA domains are related by mirror symmetry across the

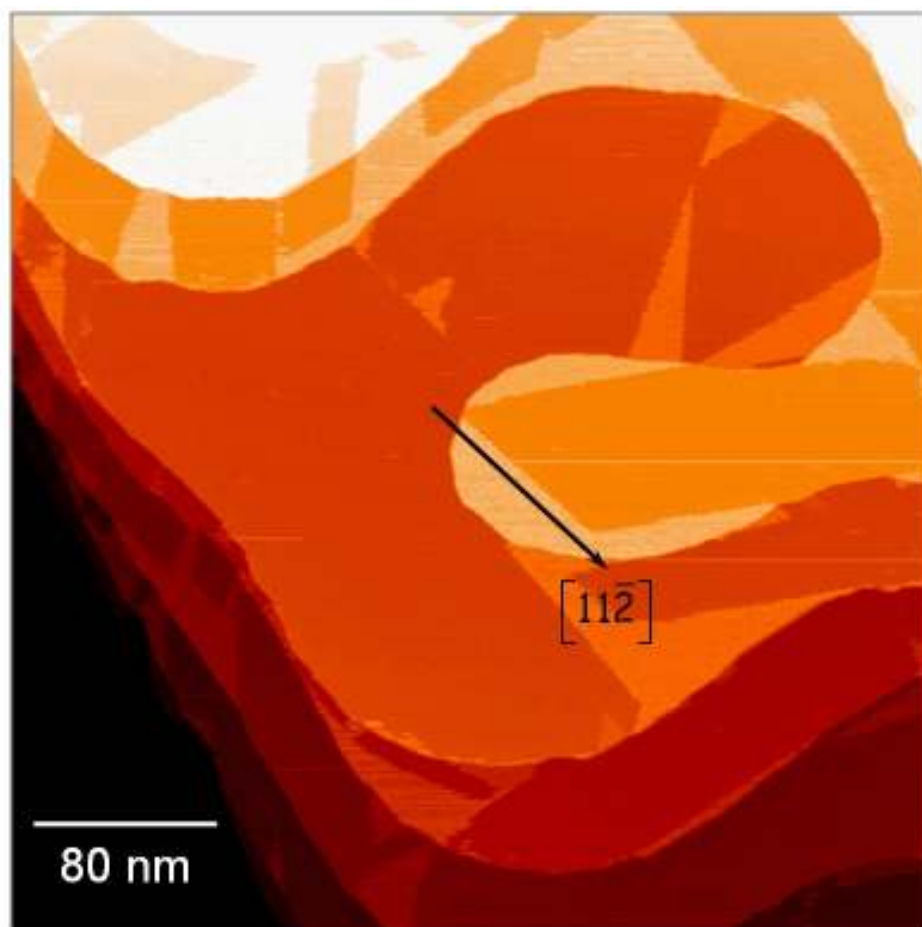


Fig. 3.2 A CCT-STM image of 0.7 ML INA on Ag(111). INA domains typically exist in rhombic shapes due to the anisotropic intermolecular interactions: the sharp boundary is along the primary H-bond direction, which is along the Ag $[11\bar{2}]$, while the noisy boundary is along the secondary H-bond direction.

Ag[11 $\bar{2}$] direction. The suggested molecular packing models are also shown in Figure 2 for these enantiomeric domains, and can be indexed as (1 -2, 3 6) and (3 2, 3 6) in matrix notation with respect to Ag(111). According to these models, each INA molecule adopts the same orientation with respect to the surface plane. Each unit cell contains two INA molecules with distinct registration with respect to the Ag(111) substrate. The INA molecules arrange in head-to-tail chains that run along the Ag[11 $\bar{2}$] direction. The chains organize into a dense 2-dimensional structure under the attraction of secondary hydrogen bonding interactions between the carbonyl oxygen of one chain and the aromatic hydrogen on the adjacent chain. The reflection-symmetry (chirality) of domains in Figure 3.3 comes from the confinement of the carboxylic acid group during the H-bond formation^{61, 62}.

In addition to these reflectional (chiral) domains, six-fold rotational domains of the INA molecular islands are also observed for each enantiomeric domain. Structural details along these rotational domain boundaries support the above structural model. Intersection of 180° rotational domains, labeled A and B in Figure 3.4, reveals how chains with opposing direction interact. Four types of domain boundaries are observed in this image. Boundary I appears as a fused “supramolecular” structure. Boundary II and III both run along the Ag[11 $\bar{2}$] direction and are molecularly sharp. However, molecules appear conjoined along Boundary II, whereas individual molecules remain distinct along Boundary III. The Boundary IV, on the other hand, exhibits a heavily kinked structure.

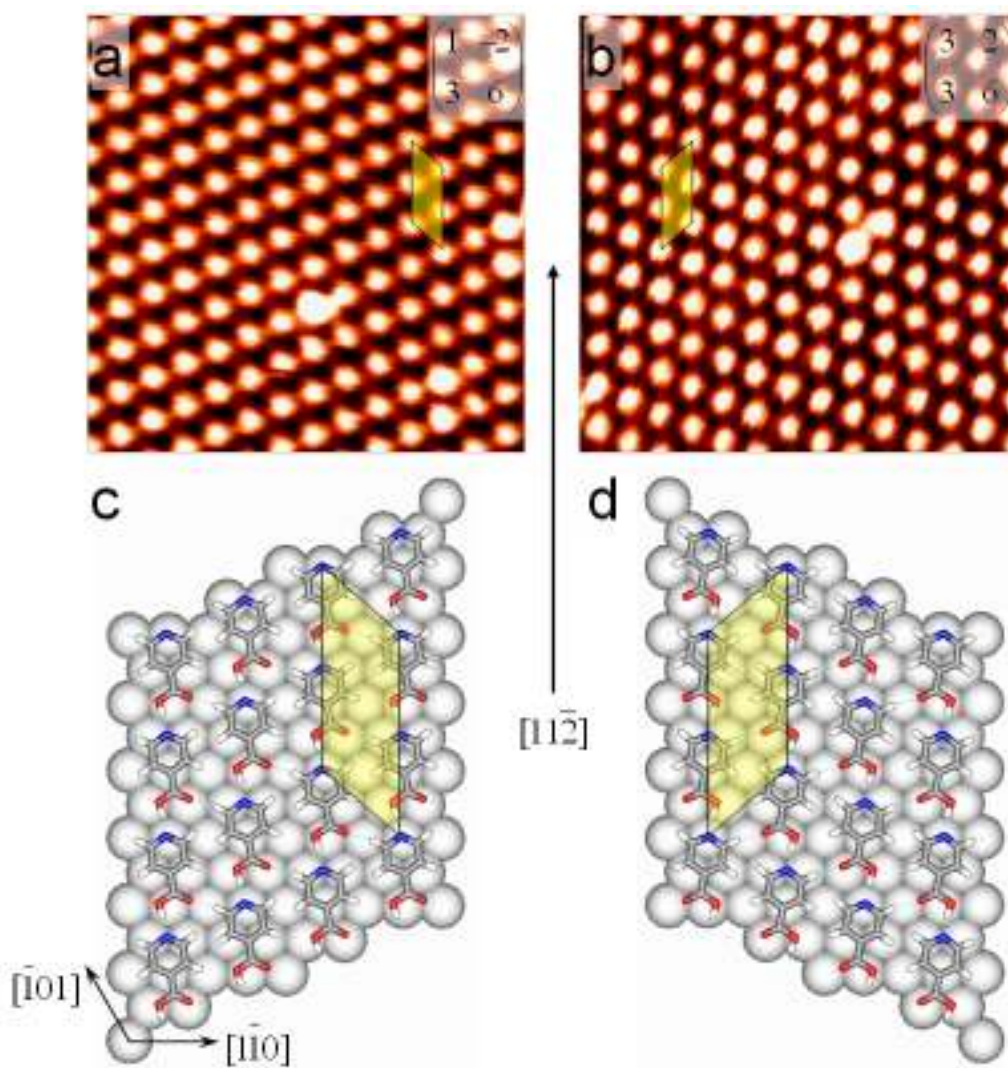


Fig. 3.3 STM images (a and b) and proposed structural models (c and d) of two INA ordered structures which demonstrate mirror symmetry with respect to the $\text{Ag}[1\bar{1}2]$ direction. For reference, a unit cell is indicated in each panel, along with the matrix notation of the domain. $\text{Ag}(111)$ lattice vectors are shown in (c). Constant-current (50 pA) STM images ($8 \times 8\text{ nm}^2$) were acquired with a -0.8 V negative sample bias.

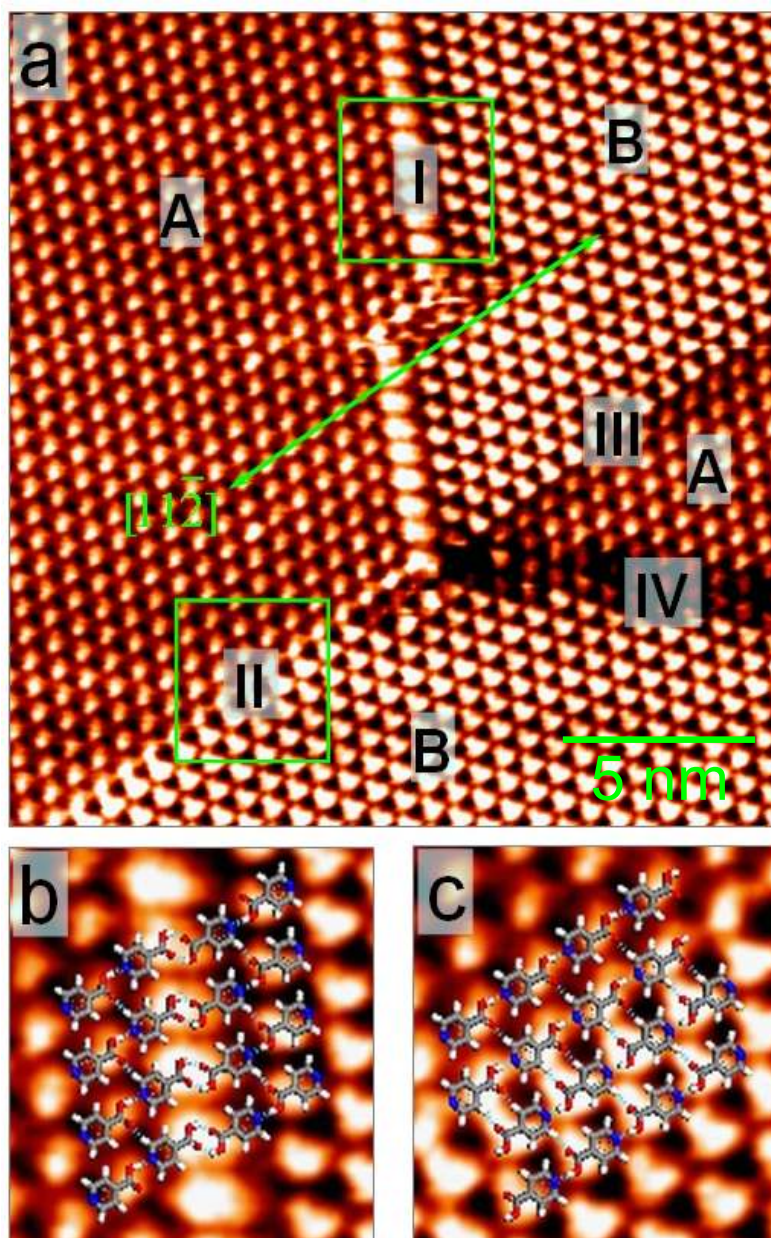


Figure 3.4 (a) An STM image demonstrating the coexistence of different INA domains on Ag(111). A and B are rotated by 180° relative to each other. (b) and (c) Magnified STM images of the boxed areas I and II in (a), superimposed with the suggested INA molecular packing models.

Models for Boundary I and II, based upon the head-to-tail INA chain structures, are given in Figure 3b and c, respectively. The fused “supramolecular” features along boundary I correspond to the fusion of adjacent INA molecules along the domain wall via the formation of carboxyl-carboxyl hydrogen bonds. This tail-to-tail hydrogen bond formation effectively terminates chain growth and stabilizes the domain wall. The molecular sized features in Boundary II, and the mild fusion between adjacent INA molecules, relates to the formation of secondary hydrogen bonds between the INA chains of opposing direction, which is absent from Boundary III.

3.3.2. XPS spectra

The distinct orientational domains of INA are accounted for with a structural model that is reminiscent of the bulk crystal structure. Within this model, INA molecules are joined in a head-to-tail hydrogen bonding arrangement. This structural model is now tested with XPS core level spectroscopy.

As anticipated for the relatively weak INA chemisorption, the Ag $3d_{5/2}$ core level is not shifted with INA deposition, and appears at the same binding energy as the clean Ag(111) film (368.4 eV). The N 1s and O 1s core level spectra of the INA film are presented in Figure 4. A least-square fitting of the N 1s spectrum with Gaussian functions located two components at 398.9 eV and 400.6 eV (Figure 3.5a). These components can be assigned to non-H-bonding nitrogen and H-bonding nitrogen, respectively^{34, 41}. The relative ratio between these two components is 2:5. Applying a similar fitting procedure to the O 1s spectrum reveals three components

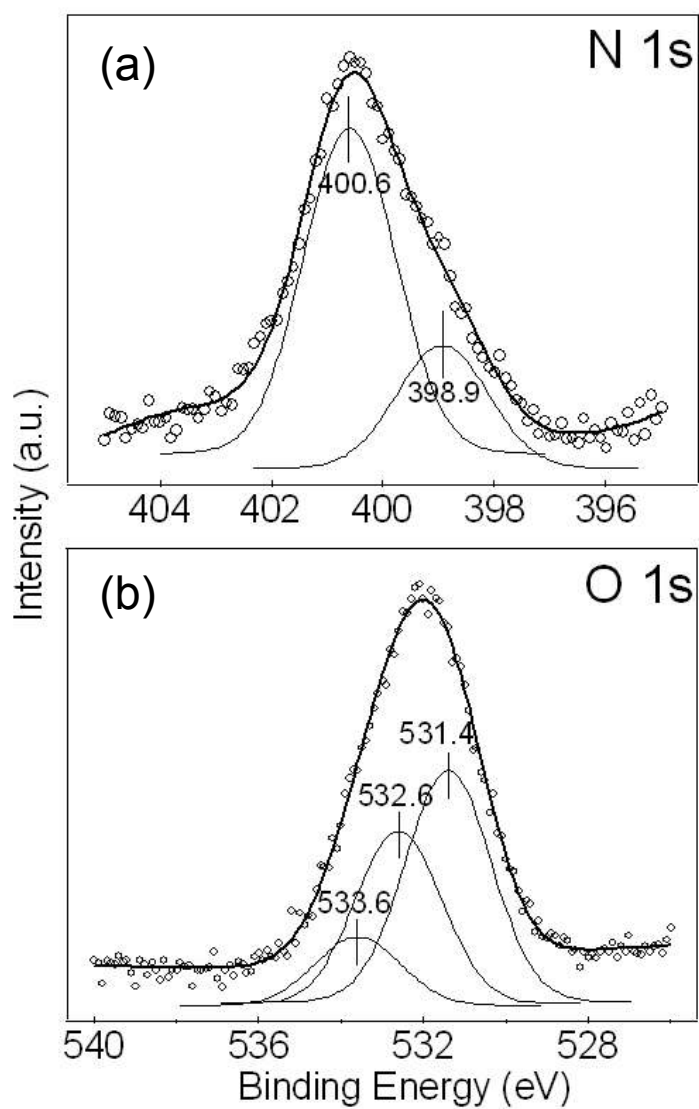


Fig. 3.5 N 1s and O 1s X-ray photoemission spectra of 0.7 ML INA on Ag(111) surface (open circles) with linear least-squares fit to Gaussian functions (line). The binding energies of the fitting components are marked in the figure.

(Figure 3.5b), with the binding energies of 531.4 eV, 532.6 eV, and 533.6 eV. These components are assigned to carbonyl oxygen, hydroxyl oxygen forming H-bond, and free hydroxyl, respectively. The relative ratio of these components is 7:5:2.

The XPS spectra of N 1s and O 1s are consistent with each other, and corroborate the STM results. The dominant H-bond motif is the head-to-tail H-bond between the ring nitrogen atoms and the hydroxyl hydrogen atoms. Approximately 30% of the INA molecules do not exhibit core-level shifts characteristic of the head-to-tail H bonds. This is attributed to the coexistence of a two-dimensional INA gas on the Ag substrate. A similar case was reported for acridine carboxylic acid. The formation of the secondary H-bond between carbonyl oxygen and aromatic hydrogen, which is clearly evident in the structural models for the commensurate structures, cannot be detected in the XPS results. This weaker hydrogen-bonding interaction may simply produce too small an energy shift for the carbonyl oxygen to permit observation.

3.4. Discussion

We have observed that head-to-tail hydrogen bonds provide a powerful organizing element for the surface-confined INA. At room temperature and coverages exceeding 0.5 ML, INA molecules readily arrange into large two-dimensional islands on Ag(111). The proposed structural model for these INA islands, shown in Figure 2, may be described as an INA molecular sheet. The sheet consists of a layer of molecules with aromatic rings parallel to the surface plane, and organized by hydrogen bonds into a two-dimensional network. The primary head-to-

tail H-bonds link molecules into long chains along the $\text{Ag}[11\bar{2}]$. A secondary hydrogen bonding interaction, which links the carbonyl oxygen of one INA chain with the aromatic hydrogen on an adjacent chain, then weaves parallel INA chains into 2-dimensional islands. These two hydrogen bonding interactions account for the rhombic shapes of INA molecular islands. The directions of these primary and secondary hydrogen bonds provide the straight edges and 131° angle of the rhombic islands.

The commensurate INA superstructure is described in matrix notation as $(1 \ -2, \ 3 \ 6)$ and its $[11\bar{2}]$ -reflected enantiomer as $(3 \ 2, \ 3 \ 6)$. Each unit cell contains two INA molecules with distinct adsorption sites and a packing density of one INA per six Ag surface atoms. The 2-D molecular packing density supports a model in which INA molecules are adsorbed with the aromatic ring parallel to the surface. This model yields primary head-to-tail hydrogen bond lengths of 0.16 nm (O-H \cdots N) and secondary hydrogen H-bond lengths of 0.21 nm (C-H \cdots O). Within the 2-D INA films, the primary H-bond direction is at an angle of 131° with respect to the secondary H-bond direction.

The distinct orientational domains, as well as the detailed structure along the domain boundary, strongly support the suggested structural model in Figure 2. XPS core level spectra further confirm the development of a head-to-tail hydrogen bonding motif upon INA island formation. The large N 1s core level shift from 398.9 eV to 400.6 eV upon INA island formation corresponds to the partial electron transfer from nitrogen atom to hydrogen atom upon the head-to-tail H-bond formation.

This two-dimensional INA structure may be compared to the bulk crystal structure of isonicotinic acid. Within the solid state, INA molecules arrange in a π -stacked INA sheets, which closely resemble the molecular film architecture observed here. Like the adlayer film, the bulk sheets are stabilized by primary head-to-tail hydrogen bonds (O-H \cdots N) and weaker secondary hydrogen bonds (C-H \cdots O). Based upon the STM and XPS studies, the INA adlayer film on Ag can be viewed as a single layer of INA(100) of the crystal, deformed to register to the Ag(111) substrate. To form this commensurate structure, the INA films must undergo a 0.4% expansion along INA[010] and a 1.3% expansion along INA[011]. In the bulk crystal, the angle between the primary H-bond direction and the secondary H-bond direction is 129.5°, compared with 131° in the INA film. Evidently, the energetic cost for this sheet deformation is compensated by the energy gain of INA chemisorption and registration to the Ag(111) substrate.

The 2-D molecular packing density of the deformed INA monolayer is virtually unchanged from the molecular sheets in the crystalline solid. To achieve registration with the substrate, the 0.747 nm molecular separation along the chain for the crystal increases to 0.750 nm. The INA chain separation is almost the same for the crystal (0.580 nm) and for the monolayer (0.578 nm). The length of the primary (head-to-tail) hydrogen bond is expanded from the crystal values of 0.151 nm to the monolayer values of 0.16 nm. The lengths of the secondary H-bond are 0.246 nm in crystal and 0.21 nm in film. However, these differences of H-bond lengths may be exaggerated by the proposed structural model. We assumed a 0° dihedral angle between the plane of the pyridine and the carboxyl group (from PM3 geometry

optimization), while a 2° dihedral angle is used for INA crystal. Moreover, the aromatic ring shape of the molecular may change upon chemisorption.

Finally, in our 2-D structural models for INA molecular films we have assumed that the INA aromatic rings lie parallel to the Ag(111) substrate. The STM provides an accurate measure of the 2-D packing density, with the tilt angle revealed only indirectly. A possible tilt of INA molecules on the Ag surface would change the length of H-bonds. Additional probes of surface structure are needed to refine the INA molecular film geometry, particularly with regard to the molecular orientation.

3.5. Conclusion

The self-assembly of isonicotinic acid on Ag(111) surface has been investigated by STM and XPS at room temperature. The 2-D molecular film arrangement is described by a structural model that involves two types of hydrogen bond interactions. A primary head-to-tail coupling between the carboxyl hydrogen and ring nitrogen links the INA molecules into chains, while a secondary interaction between the carbonyl oxygen and aromatic hydrogen drives lateral chain assembly. This 2-D film structure is reminiscent of the molecular planes of the bulk solid, but is slightly deformed for registration with the underlying Ag(111) substrate.

The complex INA film mosaic consists of two $[11\bar{2}]$ -reflection domains (enantiomers) and six 60° rotational domains for each enantiomer. Domain sizes of the order of 100 nm are commonly observed. Intersecting domains exhibit supramolecular features due to hydrogen bond formation along the domain boundary.

The domain architecture reflects the intrinsic stress of the INA molecular film and the hydrogen-bond stabilization of domain walls.

Chapter 4

Layer Dependent Isonicotinic Acid Architecture on Ag(111)

4.1 Introduction

Organic molecular films are employed in a variety of practical devices that include transistors^{63, 64}, photovoltaic cells^{59, 65, 66}, and light emitting diodes^{67, 68}. The structure of organic molecular films, particularly at the molecule-substrate interface, is thought to have a critical impact on device performance. Understanding factors that control molecular orientation and film stability at interfaces is thus an important research goal.

Recently, we have been investigating the molecular films produced by depositing N-heteroaromatic carboxylic acid on Ag(111)^{36, 37, 62, 69}. These systems are particularly interesting cases because the orientational-dependent molecular interactions might be expected to produce a variety of monolayer architectures which could be accessible through different processing conditions. In the case of the larger aromatic (9-acridine carboxylic acid), we observed how different hydrogen bonding motifs could be selected via surface morphology³⁶ and via coverage³⁷.

In the case of the smaller isonicotinic acid molecule, however, we observed only a single monolayer architecture⁶⁹. From STM measurements we derived a structural model in which INA are arranged in molecular sheets reminiscent of the structure of molecular planes in the crystalline solid. Like the bulk, INA molecules in the film are in a chain-like arrangement in which the carboxylic acid of one INA molecule forms an H bond to the ring nitrogen of its neighbor. These head-to-tail

chains are then laterally joined by secondary H bonds between carbonyl oxygen and ring hydrogen.

This structural model shows clear similarities between the INA molecular films and the bulk solid. However, the chemical interaction between the Ag(111) surface and the INA molecular film must cause deviations between the structure of the INA molecular film and the molecular solid. From a device perspective, the molecular orientation is a critical structural parameter. Unfortunately, while STM provides a very accurate measure of film periodicity, it is not a good measure of molecular orientation. STM senses molecular orientation rather indirectly from models based upon the 2-D packing densities. Based upon the STM structural measurements, we are only able to reliably estimate molecular orientation to within about 20°. Moreover, because our STM studies were limited to room temperature measurements, we could only determine the orientation of the first monolayer of film. Consequently, we could not investigate the layer-dependence of molecular orientation.

In this chapter, we utilize reflection absorption infrared spectroscopy (RAIRS) to probe the orientation of INA monolayer and multi-layer films. RAIRS is an ideal structural probe for INA molecular films for two reasons. First, RAIRS is a completely nondestructive probe and is thus well suited to the characterization of molecular films such as INA, which are easily damaged by X-rays and charged particles. Secondly, because RAIRS is a local probe it is well suited to characterizing the structure of molecular films such as INA that exhibit a variety of rotational and reflection domains.

RAIRS gains its structural sensitivity from the well-known surface selection rules. On metallic surfaces, only vibrational modes possessing a transition dipole moment component perpendicular to the substrate surface will be observed⁷⁰. Thus the relative intensities of the vibrational modes of the chemisorbed molecules provide a direct measure of surface orientation. Reflection absorption infrared spectroscopy is broadly used in determining the orientation of adsorbed molecules relative to the surface^{44, 71-75}. As a case in point, RAIRS determined the tilt angle of alkane thiol films self assembled Au(111) surfaces to be 34° from the surface normal^{76, 77} and was subsequently confirmed by both helium diffraction⁷⁸ and X-Ray Scattering measurements^{79, 80}.

In the present study, we utilize RAIRS to explore the orientation of INA molecular films in both the monolayer and multilayer regimes. We determine the orientational differences between the first layer (10° tilt) and second layer (30° incline). We describe how the first monolayer of INA molecules acts as a structural buffer between the Ag(111) substrate and the thicker film.

4.2. Experimental

This study was performed in a home built UHV system with a base pressure less than 2×10^{-10} torr. The system is coupled to a commercial FTIR spectrometer (Nicolet Nexus 670) via differentially pumped KBr windows. RAIRS spectra were typically recorded by co-addition of 512 scans at 4 cm^{-1} resolution with a high resolution mercury cadmium telluride (MCT) detector. A spectrum of clean Ag(111) was used as background. The UHV system is also equipped with a quadrupole mass

spectrometer for residual gas analysis and a Cylindrical Mirror Analyzer for Auger electron spectroscopy.

The Ag(111) substrates are ca. 700 nm films grown by physical vapor deposition on mica discs in a separate vacuum system, as previously described⁶⁹. Films were then loaded into the measurement chamber, where they were cleaned by repeated cycles of Argon ion sputtering (1kV, 0.5 μ A) and annealing (800 K). We have previously showed that these silver films are single crystalline and of (111) orientation, as demonstrated by hexagonal LEED patterns. Scanning tunneling microscopy measurements indicate the substrates are atomically smooth, with typical terrace widths of 100 nm.

INA (Aldrich, >99% purity) was physical vapor deposited on Ag(111) from a commercial Knudsen Cell evaporation source (SPECS NATC). The cell was positioned at normal incidence and a distance of 20 cm from the 100 mm x 6 mm Ag film. Before deposition, the INA was degassed in the cell for a period of four hours at 335 K. Since the sticking coefficients vary with substrate temperature, different deposition conditions were used on cold and ambient substrates, respectively. For room temperature substrates, Knudsen Cell temperatures of 390 K and exposure times of 20 minutes were used to generate monolayer films. For substrate temperatures of 125 K, a Cell temperature of 350 K and exposure times of 500 s were used to generate monolayer films.

Previous STM measurements had demonstrated that a monolayer of INA on Ag was achieved for one INA molecule per six Ag surface atoms⁶⁹. In the present study, the integrated vibrational band intensity provides a convenient measure of

surface coverage. This intensity displays a characteristic break in slope with respect to coverage upon formation of a monolayer.

To interpret the infrared spectra, vibration spectra for the free molecule and dimers in both the head-to-tail and tail-to-tail geometries were calculated with Gaussian⁸¹. The free molecule calculations were performed at the B3PW91 level with the 6-311++G** basis set. Dimer calculations were performed at the lower UHF/6-31(d) level to assess hydrogen bond induced shifts in vibrational modes.

4.3. Results

A series of coverage-dependent RAIRS spectra of isonicotinic acid adsorbed on clean Ag(111) surface at room temperature are shown in Fig. 4.1. For coverages less than 0.3 ML, a single 861 cm^{-1} peak can be distinguished from the noise. At 0.3 ML, three peaks emerge: a sharp band at 1412 cm^{-1} and two broad bands at 1120 cm^{-1} and 1710 cm^{-1} , respectively. These bands intensify with increasing exposure as the monolayer is produced. An abrupt increase in the spectral complexity at an exposure time of 10 minutes indicates the onset of multilayer formation. The multilayer film shows the same spectral signature as the condensed phase INA spectrum. (Reported in Aldrich library). In particular, vibrational bands at 1710 cm^{-1} and 2350 cm^{-1} for the multilayer film exhibit intensities and band shapes characteristic of the INA solid.

Monolayer films were also produced by evaporation onto cold Ag(111) substrates. Figure 4.2 shows the RAIRS spectra of INA adsorbed on Ag(111) at 135 K. The spectra display the same set of bands as in Fig. 4.1. However, there are key differences involving two vibrational bands. As shown in Fig. 4.3, 1120 cm^{-1} feature

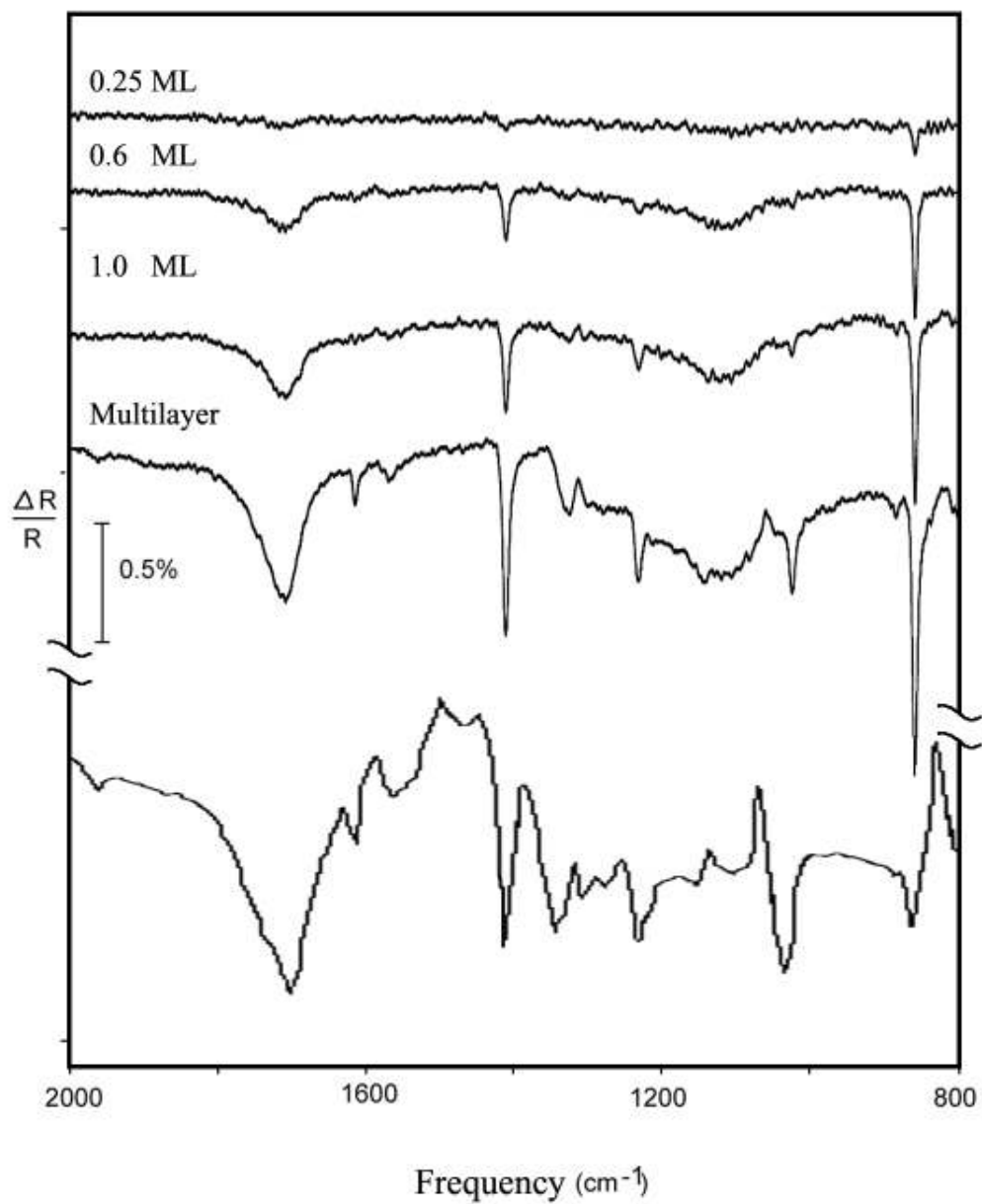


Fig. 4.1 RAIR spectra of isonicotinic acid adsorbed on Ag(111) at room temperature. The coverage is (from top to bottom): 0.25ML, 0.6ML, 1ML and multilayer. IR spectrum of INA bulk crystal is also included at the bottom.

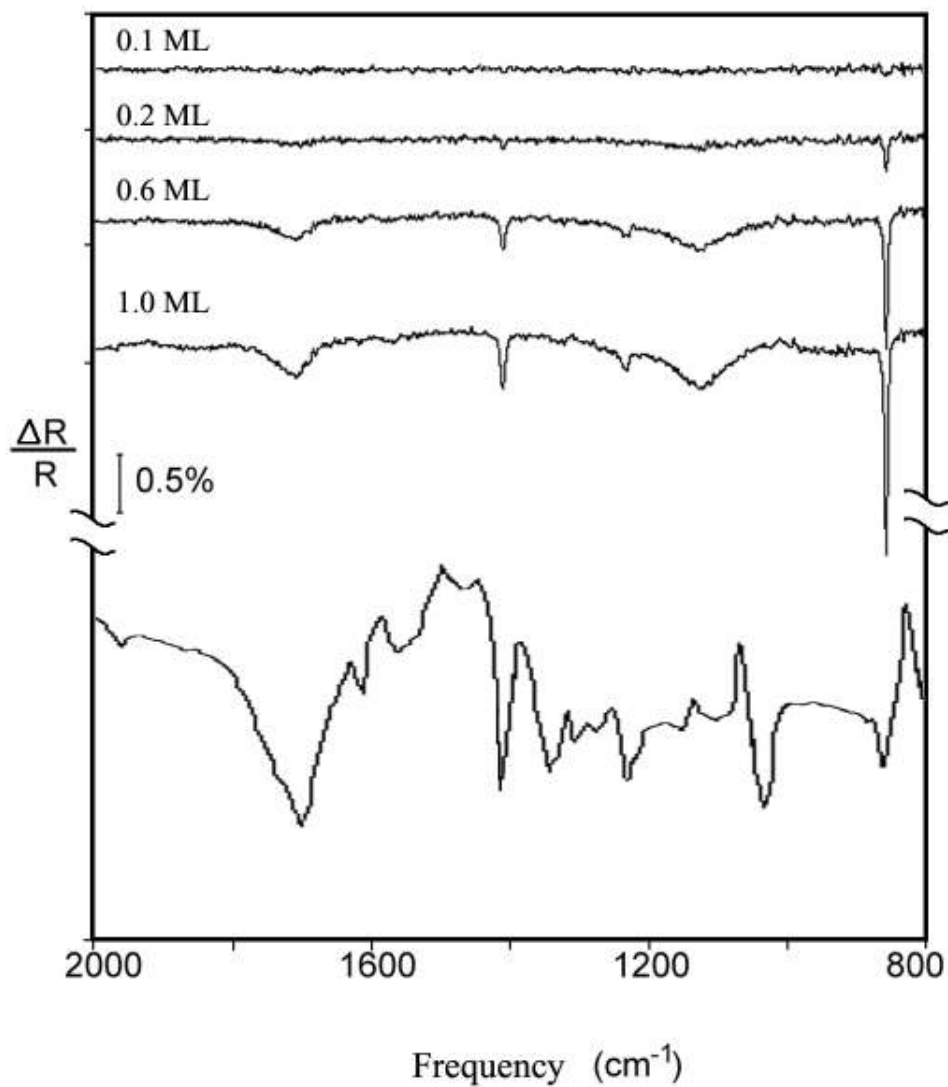


Fig. 4.2 RAIRS spectra of isonicotinic acid adsorbed on Ag(111) at 135 K. The coverage is (from top to bottom): 0.1ML, 0.2ML, 0.6ML and 1.0 ML. A IR spectrum of INA bulk crystal is included at the bottom.

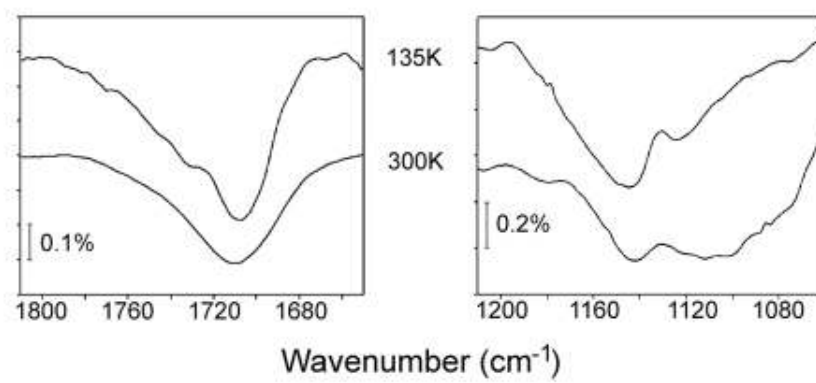


Fig. 4.3 RAIRES spectra of 1 monolayer of INA adsorbed on Ag(111).

shifts to 1153 cm⁻¹ upon cooling, and in the carbonyl region, the 1710 cm⁻¹ band exhibits 1734 cm⁻¹ shoulder and a weak 1772 cm⁻¹ peak.

To interpret these vibrational measurements, theoretical calculations were performed at two different levels: B3PW91/6-311++G** and UHF/6-31(d). With 14 atoms, the free INA molecule exhibits 36 fundamental vibration modes in gas phase. Hydrogen bond formation makes the spectra more complex. The higher level DFT (B3PW91/6-311++G**) calculation is only performed for the monomers. The lower level UHF calculation is performed for the monomer, head-to-tail dimer and tail-to-tail dimer. Although UHF calculations performed at this level are not accurate in determining hydrogen bond strengths, they can predict characteristic frequencies for different H-bond configurations. Consequently, they provide insight and guidance in distinguishing the types of the hydrogen bonds.

For theoretical calculations, there are always systematical errors. Thus, the computational results need to be scaled for comparison with the experimental data. Palafox performed theoretical calculations at a range of levels and determined linear scaling formulae for different levels of theory.⁸² Rode et al. subsequently published the scaling formula for B3PW91/6-311++G**.⁸³

$$\nu_{\text{scaled}} = 0.955 * \nu_{\text{calculated}} + 25.7 \text{ cm}^{-1} \quad (1)$$

This equation provides excellent agreement with the experimental data (< 10 cm⁻¹ error for most stretch modes) for measured isonicotinic acid molecular vibrations.⁸⁴

We adopt this scaling formula for our INA films. In Table 4.1, the experimental values for the INA films and the calculated (scaled) frequencies for the INA monomer are listed.

The UHF computational results for the monomer and dimers were scaled by a factor of 0.88, which is deduced from a comparison of the results of nicotinic acid to the experimental infrared vibrational results of gas phase nicotinic acid. These UHF results are presented in Table 4.2.

4.4. Discussion

We begin with an assignment of the four observed vibrational modes that dominate the monolayer RAIRS spectrum. Direct comparison of the measured values with the scaled computation results leads to the following assignments: The sharpest peak at 861 cm^{-1} (FWHM 6 cm^{-1}) is assigned to the C-H out-of-plane bending mode of the aromatic ring (monomer (m) mode 14). The broad 1120 cm^{-1} (90 cm^{-1} FWHM) feature involves bending motion of O-H (m mode 22) and C-H (m mode 23). The relatively sharp 1412 cm^{-1} band (10 cm^{-1} FWHM) is assigned to the C-C in-plane scissoring mode of the aromatic ring (m mode 24). The broad 1710 cm^{-1} band, with a FWHM $>60\text{ cm}^{-1}$, is assigned to C=O stretch (m mode 31) within a complex chemical environment.

The vibrational spectra confirm that INA adsorbs molecularly on Ag(111) without deprotonation. Deprotonation would lead to the formation of the carboxylate moiety and a characteristic carboxylate band, $\nu_s(\text{OCO})$, at 1400 cm^{-1} . The absence of this carboxylate feature and the presence of the 1120 cm^{-1} band, assigned to the deformation of O-H, provide clear evidence for molecular INA. Not surprisingly, the multilayer film also displays molecular adsorption: At coverages exceeding 1 ML, a pronounced mode at 1325 cm^{-1} , representing $\beta(\text{O-H})$ (m mode 26), is evident. We

No.	Theoretical		Experimental		Description
	B3PW91/6-311++G** (cm ⁻¹)	UHF/6-31(d) (cm ⁻¹)	300K(cm ⁻¹)	135K(cm ⁻¹)	
14	854	849	861	861	γ(CH)
15	883	879	884	894	γ(CH)
16	970	963			γ(CH)
17	986	975			γ(CH)
18	994	996			ν(C=C)
19	1065	1021	1024	1029	β(CH)
20	1079	1039			β(CH)
21	1105	1082			β(CH)+ ν(CO)
22	1176	1109	1120	1131	β(OH)
23	1214	1180	1144	1152	β(CH)
24	1276	1189	1231	1237	β(OH)+ν(C=C)
25	1311	1299			β(CH)
26	1341	1339	1329	1334	β(OH)
27	1402	1383	1412	1412	ν(C=C)
28	1481	1479			ν(C=C)
29	1573	1563			ν(C=C)
30	1599	1598	1615	1616	ν(C=C)
31	1761	1783	1710	1710, 1772	ν(C=O)
32	3047	2971			ν(CH)
33	3051	2974			ν(CH)
34	3096	3011			ν(CH)
35	3102	3013			ν(CH)
36	3649	3569	2350	2398	ν(OH)

Table. 4.1 Scaled calculation results of INA monomer with assignments. The experimental results on cold and room temperature substrates are included.

Experimental		Theoretical		
300K	135K	Monomer (cm ⁻¹)	T-T dimer (cm ⁻¹)	H-T dimer (cm ⁻¹)
861	861	849	858	855
884	894	879	880	880
1024	1029	1021	1021	1024
1124	1153	1109	1111	1107
1231	1237	1189	1186	1180
1325	1334	1339	1376	1340
1412	1412	1383	1389	1386
1615	1616	1598	1598	1606
1710	1710, 1772	1783	1740	1787, 1756

Table 4.2 The experimental results compared with scaled calculated (UHF/6-31(d)) vibrational spectra of isonicotinic acid monomer, head-to-tail (H-T) dimer and tail-to-tail (T-T) dimer.

thus determine that deprotonation does not occur on the room temperature substrate. This result is consistent with previous studies of deprotonation of carboxylic acids on silver substrates. Parker *et al.* reported that at ambient temperature, benzoic acid only deprotonates on preoxidized Ag(110) and Ag(111) surfaces³⁸. Larger carboxylic acid molecules such as 4-[trans-2-(pyrid-4-yl-vinyl)]benzoic acid (PVBA) and 4-[(pyrid-4-yl-ethynyl)]benzoic acid (PEBA) also adsorb molecularly on Ag(111) at room temperature²⁴.

The vibrational spectra also report on hydrogen bond formation between INA molecules. Quantum chemistry calculations predict a red shift in the carbonyl stretch from the free molecule (1783 cm^{-1}) upon dimer formation in either the head-to-tail (1756 cm^{-1}) or tail-to-tail (1740 cm^{-1}) configuration. The 1710 cm^{-1} C=O stretch that we observed from the ordered monolayer films (300K result) significantly exceeds the dimer values. This giant red shift is accounted for by the well-known cooperative effect for extended hydrogen bonded systems^{34, 85-87}.

The carbonyl band shape for the film grown at 135 K displays multiple components. Based upon the reduced INA mobility at 135 K, we expect the film to include a mixture of monomers, small aggregates (include short head-to-tail chains and tail-to-tail bonded structures) and long chains. The trace peak at 1771 cm^{-1} is assigned to the INA monomer and the substantial 1740 cm^{-1} shoulder to small aggregates.

The structural difference between the films grown on the 135 K and 300 K substrates are further supported by the O-H deformation mode. The β (O-H) feature

shows an increasing intensity and a significant red shift at 300K, as expected for the head-to-tail network.

We next analyze the band intensities for molecular orientation. The free INA molecule has 36 normal modes of vibration, of which 23 should fall within our experimentally accessible region ($800 - 4000 \text{ cm}^{-1}$). In the surface infrared measurements at submonolayer coverages, we observe only four significant infrared vibrational bands. This spectral simplification is largely due to the well-known surface infrared selection rule: only vibrational modes having a transition dipole moment component perpendicular to the substrate surface will be observed. It is instructive to classify the normal modes as follows: in-plane modes possess transition dipole moments that are parallel to the aromatic plane; out-of plane modes possess transition dipole moments that are perpendicular to the molecular plane.

The two sharpest bands in the submonolayer spectra are found to be an out-of-plane mode (C-H bending mode at 861 cm^{-1}) and a (mostly) in-plane mode (C-H scissor mode at 1412 cm^{-1}), as depicted in Fig. 4.5. At the lowest coverage, the out-of-plane 861 cm^{-1} band dominates the spectrum, indicating that the molecule is \sim parallel to the metal surface. Beginning at 0.3 ML coverage, the appearance of the in-plane 1412 cm^{-1} mode shows that the molecules must be tilted with respect to the surface plane. Based upon the relative intensities of these two modes, the tilt angle must be relatively small.

The average molecular orientation with respect to the surface plane can be calculated using the relative intensity of selected modes. The integrated area of an infrared band can be written as⁷¹:

$$A(i) = \frac{32\pi^3 n}{hca} M_{iz}^2 \nu_{i0} G(\theta) \quad (2)$$

Where A is the integrated area of selected vibration mode, n is the number of the dipoles, h is Planck's constant, c is the speed of light, a is the surface area, M is the transition dipole moment component in the direction of the surface normal, ν is the resonant frequency, and G(θ) is a function that depends on the angle of incidence and the dielectric constant of the substrate and is only weakly dependent to the frequency. In a given sample, a and G(θ) can be treat as constants. Therefore, the formulation can be simplified as:

$$A(i) = C \times n \nu_{i0} M_{iz}^2 \quad (3)$$

If we know the angle (φ) between transition dipole moment and the surface plane, then the magnitude of M can be described as:

$$M_{iz} = M_i \times \sin(\varphi) \quad (4)$$

Combining Eqns. (3) and (4), we get:

$$A(i) = C \times n \nu_{i0} M_i^2 \sin^2(\varphi) \quad (5)$$

To study the orientation of INA molecules on Ag(111) surface, we compare the relative intensities of the two modes shown in Fig. 4.4: the C-H out-of-plane mode (with transition dipole moment $M_{861\text{cm}^{-1}}$) and the -C=C- in-plane in-phase

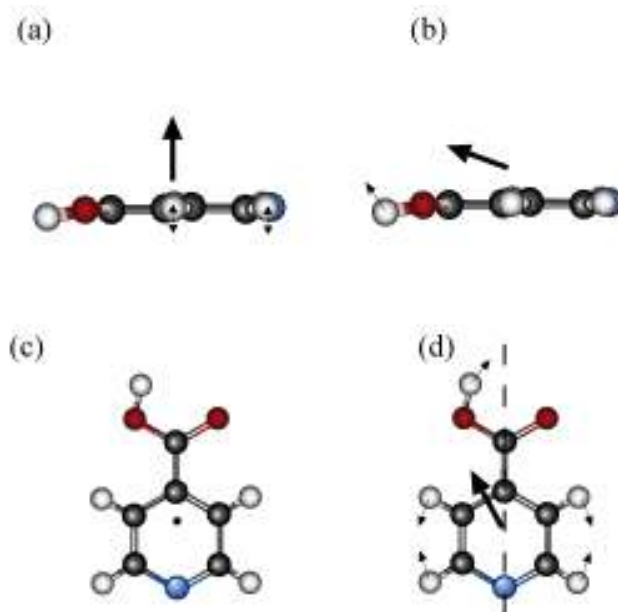


Fig. 4.4 schematic drawing of (a) side-view of out-of-plane C-H mode (861 cm^{-1}); (b) side-view of -C=C- in phase scissoring mode (1412 cm^{-1}); (c) top-view of 861 cm^{-1} mode; (d) top-view of 1412 cm^{-1} mode. The transition dipole moments are illustrated as bold arrows.

bending mode (with transition dipole moment $M_{1412\text{cm}^{-1}}$ directed 20° away from the aromatic plane). These two modes are chosen because they are not directly involved in hydrogen-bond formation.

Assuming C is the same for both modes and the angle between the molecular plane and the substrate is α ,

$$\frac{A_{861\text{cm}^{-1}}}{A_{1412\text{cm}^{-1}}} = \frac{861 \times M_{861\text{cm}^{-1}}^2 \sin^2(90^\circ - \alpha)}{1412 \times M_{1412\text{cm}^{-1}}^2 \sin^2(20^\circ + \alpha)} \quad (6)$$

The coverage dependence of the orientation may be determined with Equation (6). Figure 4.5 plots the integrated intensity ratio of the C-H out-of-plane bending mode (861 cm^{-1}) and the -C=C- in-plane bending mode (1412 cm^{-1}) at room temperature as a function of coverage. Corresponding tilt angles for each coverage are determined from Eqn. (6) and included on the diagram. At submonolayer coverages, the intensity ratio increases from 0.3 to 0.4 as the monolayer develops, corresponding to an average incline angle that increases from 5° at 0.2 ML to 10° at a coverage of 0.8 ML. We estimate an uncertainty of $+2^\circ$ in the determination due to the uncertainty in the intensity ratio. For coverages exceeding one monolayer, the intensity ratio increases markedly, indicating a sudden increase in the average incline angle to 20° for the bilayer film. Once the bilayer is established, the intensity ratio increases more slowly to indicate an average angle of 23° for the trilayer.

To interpret the increase in the average angle in the 0.2 ML (5°) to 0.8 ML (10°) range, we refer to the structure of INA submonolayer films, determined by STM. At 0.2 ML INA exists on the surface as a 2-D gas. The 5° angle corresponds to the average orientation of freely diffusing INA. At 0.8 ML, the surface is covered

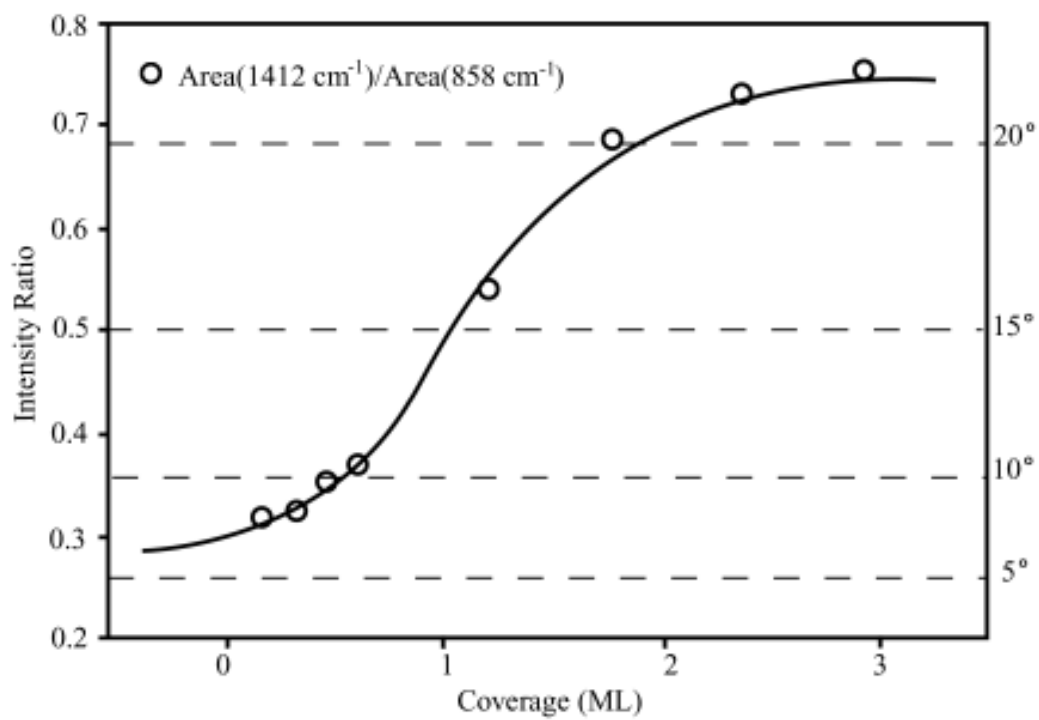


Fig. 4.5 The ratio of integrated IR absorption intensity of 1412 cm^{-1} band to 858 cm^{-1} band versus the isonicotinic acid coverage adsorbed on Ag(111) at room temperature.

by large islands, in which INA molecules are linked by 2-D hydrogen bonding networks. Evidently, the INA molecules must be inclined from the surface by 10° in order to form the hydrogen bonding network.

The average orientation angles for the multilayer films reflect the contribution of all three layers. If we assume that the first monolayer angle (10°) does not change upon formation of subsequent layers and each layer contributes equally to the average, we extract a second layer angle of 30° and a third layer angle of 29° . The common $\sim 30^\circ$ incline for the 2nd and 3rd INA layer suggests that the aromatic rings of the INA molecules are parallel and of different orientation than the first monolayer.

Crystalline INA is a layered solid with parallel planes of aromatic rings. The layers are constrained by π - π interactions. The parallel stacking of the second and third layer of the INA films thus reproduces the stacking for the bulk crystalline solid. The distinct orientation of the first INA monolayer indicates a different “stacking” or π - π interaction. The chemical interaction between INA and the Ag substrate is the source for this distinct orientation.

We have so far determined the incline angle of INA, but have not specified the direction of incline. As shown in Fig. 6, this incline can be accomplished via a twist or tilt of the INA molecule with respect to the surface plane. Unfortunately, the transition dipole moment of the “in-plane” 1412 cm^{-1} mode (Fig. 4.4 b,d) possesses both a 20° tilt from the aromatic plane, as treated above and included in Eqn. 6, and a 20° rotation from the long molecular axis. Consequently, either tilting or twisting the molecule can increase the angle between this dipole vector and the surface. The RAIRS data alone prove that INA molecules are adsorbed on Ag(111) surface with a

small incline angle, but cannot specify this inclination as tilt or twist. Based upon the following arguments, we believe that the RAIS measured incline angle represents molecular tilt for the monolayer and the combined effects of tilt and twist for the multilayer.

Previous investigations concerning related N-heteroaromatic molecules in the monolayer regime have determined tilted geometries⁸⁸⁻⁹⁰. For example, pyridine adsorbs on Ag(111) through the nitrogen lone pair, exhibiting a tilted orientation at monolayer coverages^{88, 89}. In the case of pyridine, the tilt angle represents the combined effects of chemisorption through the lone pair donation of the nitrogen atom and π interaction between the aromatic ring and substrate. INA molecules possess the similar ability for interacting with the substrate through the nitrogen lone pair and through π donation, which should produce a tilted monolayer structure. A twisted structure would further compromise hydrogen bond formation for the monolayer films.

The orientations of multilayer structures are more complex. Without the electronic perturbation and rigidity of the metal substrate, intermolecular interactions are most important for setting orientation. Nonetheless INA molecules in the second layer are unlikely to be tilted by 30°. Such a tilt would prohibitively elongate the primary head-to-tail hydrogen-bond, skew the hydrogen bond angles, and generally produce less stable structures. The multilayer structures are, however, better able to accommodate the twisting of INA molecules. Moreover, INA chains in the monolayer are slightly compressed from their spacing in the bulk and twisting will

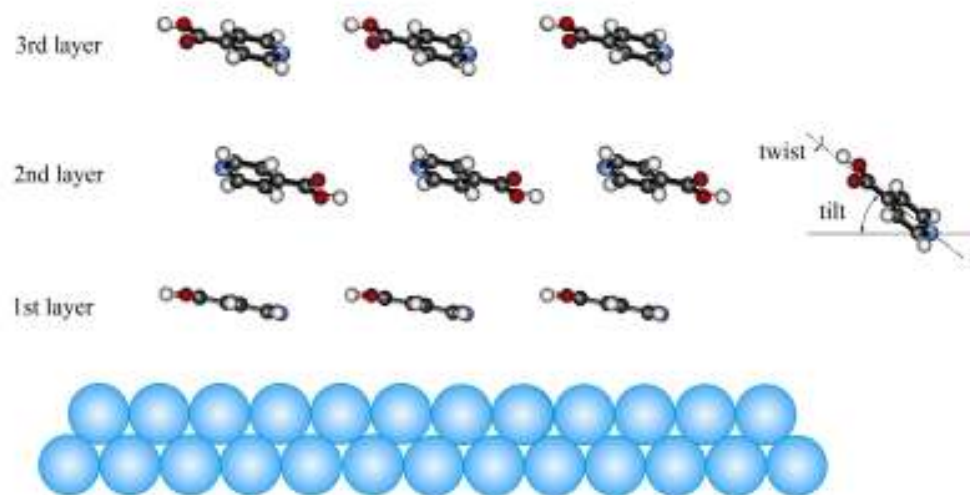


Fig. 4.6 Suggested model of layer-by-layer INA adsorbed structures on Ag(111)

relax the 2nd layer molecules to generate more stable configurations. Accordingly, a schematic model of trilayer film architecture is presented in Fig 4.6. In this model, the second layer possesses the same tilt angle as the first layer ($\sim 10^\circ$). As observed in other fused-ring systems, the second layer is unaffected by the substrate⁹¹. The relative position and the distance between adjacent layers are constrained by the π - π interaction. To compensate the mismatching of the molecular crystal lattice in the first adsorbed layer, 20° of twist is employed to increase the side-link hydrogen bond length. Although the molecules are approaching the crystal structure on the surface, the second and third layer we observed is still structurally distinct from the bulk structure. In previous studies of aromatic molecule adsorption on metal surface, a few layers of buffer are observed before molecules grow into the bulk structure⁹². Therefore, we conclude that the structure of the 2nd and 3rd layer remains a transitional structure.

4.5 Conclusion

The adsorption of isonicotinic acid ($C_6H_5NO_2$) on Ag(111) surface is studied by reflection absorption infrared spectroscopy at two distinct temperatures. At room temperature and near-monolayer coverage, the vibrational spectrum indicates a homogeneous INA film structure with extensive hydrogen bond formation. The bilayer vibrational spectrum exhibits vibrational features that are characteristic of the bulk. On the frozen substrate, the vibrational spectrum reveals a heterogeneous INA film structure that includes “free” INA molecules, hydrogen-bonded aggregates, and

island structures within the monolayer. Adsorption without deprotonation is observed at all reported temperatures.

The layer-dependent orientation of the INA films was determined from the relative intensity of select bands. Free molecules exhibit very small $\sim 5^\circ$ tilt angles. Upon island (hydrogen-bond) formation, the tilt angle increases to 10° , as the ordered monolayer is formed. Subsequent INA layers exhibit a net $\sim 30^\circ$ inclination angle, representing the combined effects of tilting and twisting. To grow into bulk-like material, at least two layers of transitional structures are necessary.

Chapter 5

H-Bond Directed Adlayer Architecture of Fused Aromatic Compounds: Contrasting AA vs. ACA on Ag(111)

5.1. Introduction

Self-assembled nanostructures supported on solid substrates provide a promising approach to microelectronic fabrication. For practical applications, a well-defined surface adlayer is substantial. Surface structure depends on the subtle balance between intermolecular and adsorbate-substrate interactions. Therefore, one way to control the size, shape and orientation of surface aggregates is by tuning interactions among the adsorbed molecules. For example, substituted porphyrin adsorption on Au(111) shows that surface aggregates vary from trimers to tetramers to one-dimensional wire as the number and position of cyano substituents change in the porphyrin.

In the last two chapters, I investigated surface structures of isonicotinic acid (INA) monolayers on Ag(111) in detail^{69, 93}. In this chapter, I expand this work to another molecule in the N-heteroaromatic carboxylic acid family: 9-Acridine carboxylic acid (ACA) (Fig. 5.1). ACA molecules have the same functionalized aromatic core as isonicotinic acid. Consequently, both the head-to-tail H-bond and tail-to-tail H-bond bonding motifs are available for ACA. Quantum chemistry calculations indicate that head-to-tail H-bonding energy is stronger than tail-to-tail H-bonding energy. X-ray diffraction measurements reveal the head-to-tail hydrogen

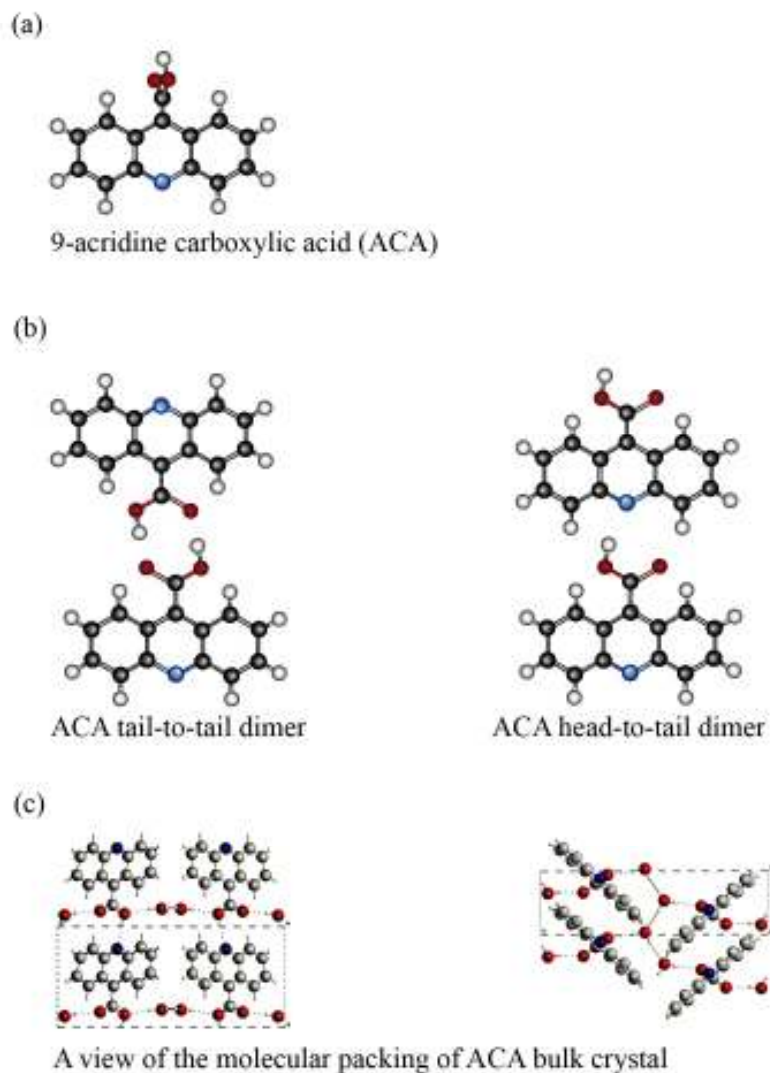


Figure 5.1 Schematic drawings of (a) ACA molecule. A dihedral angle of 78.9° is illustrated, (b) hydrogen bond arrangements, and (c) bulk crystal structure of ACA hydrate. ACA molecules are bonded by head-to-tail couplings with a twisted orientation.

bonding arrangement in dihydrate crystals of ACA⁹⁴. However, ACA possesses two more aromatic rings than INA, which significantly affects the surface structure in three ways. First, the width of this molecule prevents the formation of a secondary (side-linked) hydrogen bond. Secondly, repulsive interactions between the fused aromatic rings and the carboxylic group force the carboxylic group to rotate around the C-C bond and adopt a non-planar geometry. X-ray diffraction measurements reveal that the fused-ring is near planar, while the dihedral angle between the carboxyl group plane and ring plane is 78.1° ⁹⁴. Finally, the fused ring system has a considerably greater quadrupole moment and dispersive interaction than INA, giving rise to orientation dependent interactions. Thus, the orientation of ACA on metal surfaces can be much more complex than the simpler INA molecule with a richer coverage dependence.

To assist in the interpretation of results on this chemically complex system, two related triple-ringed systems were studied for comparison: 9-Anthroic acid (AA) (Fig 5.2) is the homocyclic version of the ACA heterocycle, in which ACA's ring nitrogen is replaced with a carbon (and terminal hydrogen). The loss of the ring nitrogen eliminates the head-to-tail hydrogen bonding motif, allowing AA to form only tail-to-tail dimers. Hence, comparative studies of the architecture of ACA and AA allow us to address the role of the ring nitrogen on supramolecular assembly.

Recently, ACA adsorption on Ag(111) at room temperature has been studied by STM and XPS^{36, 37}. Based upon the direct observation of well-ordered monolayer structures, an approximate coverage dependent phase diagram has been reported. (See Fig. 5.3) Here, we define one monolayer as one ACA molecule

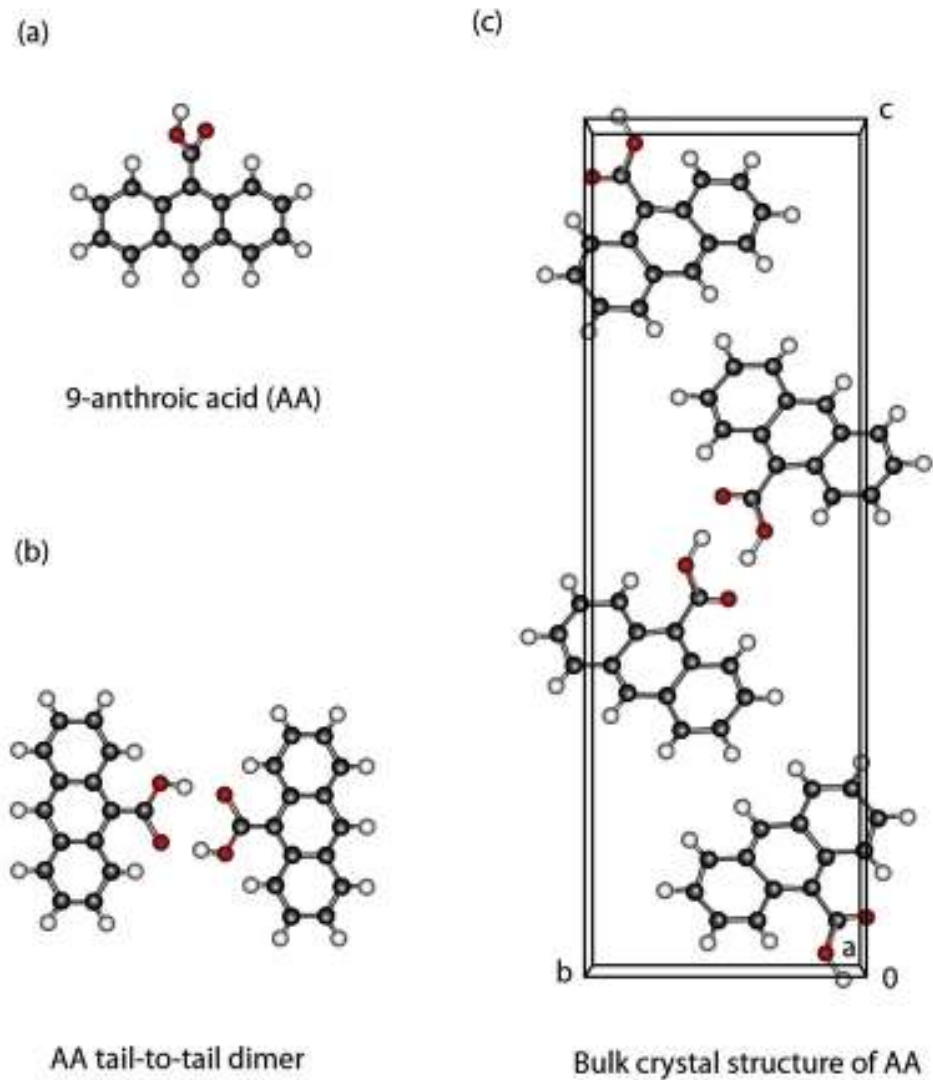


Figure 5.2 Schematic drawings of (a) AA molecule. A dihedral angle of 54° is illustrated, (b) hydrogen bond arrangement, and (c) bulk crystal structure of AA. AA molecules are bonded by tail-to-tail couplings with a twisted orientation.

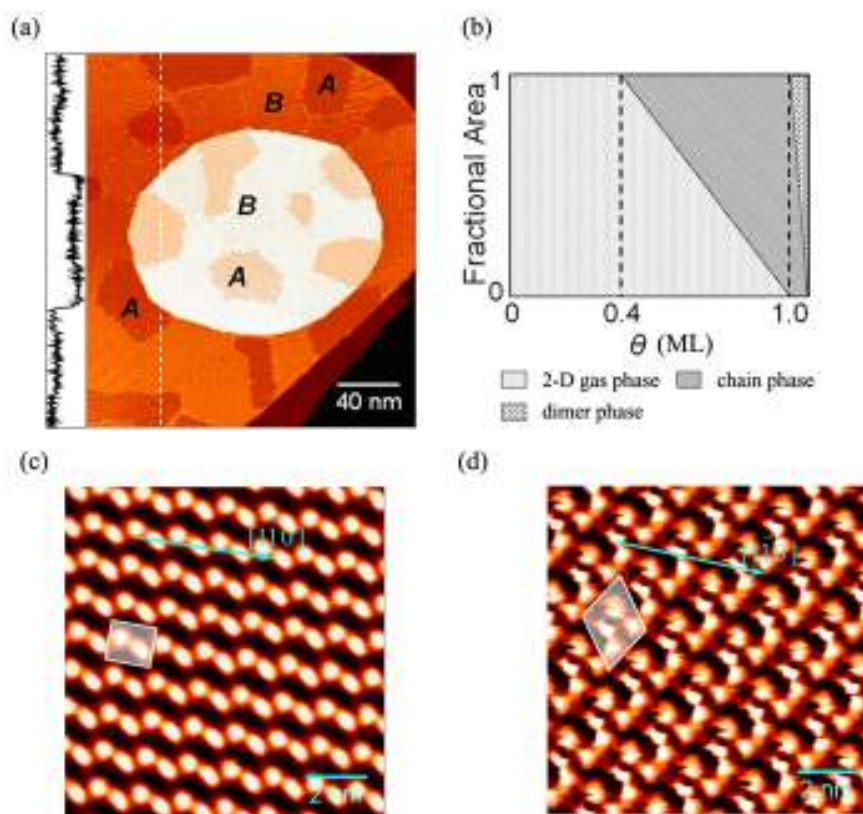


Fig. 5.3 STM images and schematic model of ACA adsorption on Ag(111) at room temperature. (a) co-existence of chain phase (A) and dimer phase (B). Molecular resolved images of (c) chain phase and (d) dimer phase are shown. A schematic compositional phase diagram is included in (b). (reproduced from JACS, **2006**, *128*, 8493)

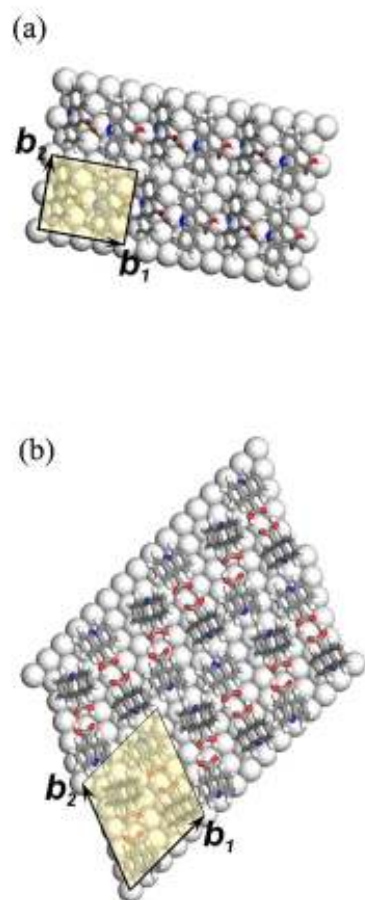


Fig. 5.4 The proposed structure model of (a) chain phase and (b) dimer phase, respectively. Unit cells are pointed out. Each unit cell of the chain phase contains two inequivalent ACA molecules. There are four molecules in each unit cell of the dimer phase. (reproduced from JACS, **2006**, *128*, 8493)

per eight silver surface atoms. At lower coverages ($\theta < 0.4$ ML), large terraces are occupied by mobile ACA. This low-coverage phase is described as a two-dimensional gas. When the ACA coverage reaches 0.4 ML, ACA islands appear. These islands continue to grow as coverage increases from 0.4 to 1 ML. The structural model proposed for this ordered submonolayer phase is a “chain model”, in which ACA molecules are arranged in head-to-tail H-bonding arrangements along $[1\bar{1}0]$. To account for the observation of two inequivalent ACA molecules per unit cell, and the density of ACA molecules, the ACA molecules are arranged with alternating incline angles, as shown in Fig. 5.4. The structural model proposes an appreciable alternating tilt ($\sim 40^\circ$) for the ACA molecules on the surface, in distinct contrast to our findings on the INA system (tilt angle of 10°). For coverages exceeding 1 ML, a second ordered phase of ACA appears. Based upon the molecularly resolved STM images, a “dimer phase” model is proposed for this structure. In this model, ACA molecules form carboxyl-carboxyl dimers with considerably large twist angles. The inclined structural models for the ACA architectures are based on the two-dimensional ACA packing density. The STM topography does not directly reveal the ACA orientation. The proposed alternative twist arrangements, with $\sim 40^\circ$ molecular tilts, demand experimental testing. We thus undertook the present RAIRS investigation of ACA monolayers to look for independent evidence of the ACA orientation and molecular architecture. The molecular arrangement provides crucial evidence for the balance of chemisorption and electrostatic forces.

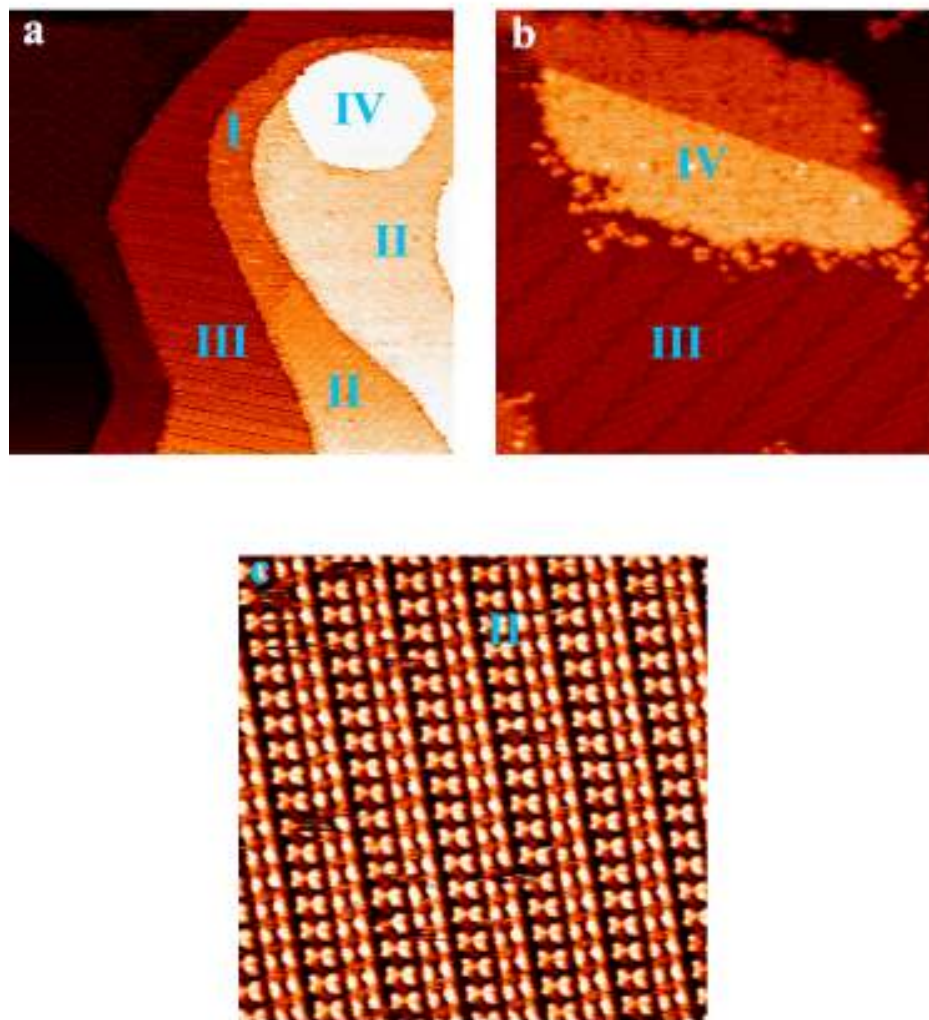


Fig. 5.5 STM images of AA adlayer structures on Ag(111) at room temperature: (a) 200 nm X 200 nm image reveals coexistence of AA phases I (2-D gas), II (1st dimer phase), III (2nd dimer phase) and IV (bilayer phase), (b) magnified image of 2nd dimer phase and AA bilayer, (c) magnified image of 1st dimer phase, showing resolution of AA dimers.

The homocyclic AA is chemically simpler than ACA, with just one H-bonding motif. The more extensive series of surface phases observed for AA in recent STM measurements is thus surprising⁹⁵. Underlying this phase behavior is a series of adlayer structures, based upon tail-tail dimers. While detailed two-dimensional models have not yet been reported for the AA phases, the packing density of the AA dimers indicate that the aromatic plane must be significantly (> 30 deg) tilted with respect to the Ag(111) plane, in all ordered phases.

In the present study we will closely compare the infrared vibrational spectra of the ACA and AA monolayers. The carbonyl stretching frequencies will provide a very sensitive measurement of the hydrogen-bonding states for the adsorbate. The relative intensities of vibrational modes will allow us to explore the orientation of the adsorbate. Reported STM studies were limited to room temperature, where ordered structures spontaneously form. We extend this study to cryogenic temperatures, where the evolution from molecular adsorbate to long range order can be investigated.

5.2. Experimental

All experimental measurements were performed on films grown in an ultrahigh vacuum system. Infrared measurements were performed in a home built UHV chamber described previously⁹³. RAIRS spectra were recorded by co-addition of 1024 scans at 4 cm^{-1} resolution. The substrates used in this study were 700 nm Ag(111) films grown on mica supports. The films were then cleaned by repeat

sputtering/annealing cycles until there were no obvious Ag-O peaks visible in the RAIRS spectra.

The organic films were made by molecular beam deposition through a commercial Knudsen Cell evaporation source (SPECS NATC). Before deposition, ACA hydrate (Aldrich, 98%) and AA (Aldrich, 99%) molecules were degassed in the Knudsen Cell for a period of 2 hours at 375K and 360 K, respectively. The deposition rate is 20 minutes for a monolayer of ACA at 420 K and AA at 400 K.

Gaussian programs at B3PW91 level combined with the 6-311++G** basis set were used to characterize the normal vibrational modes for both ACA and AA molecules, as a reference for the present work.

5.3. Results and discussion

5.3.1 Theoretical Calculation

The number of surface vibrational studies involving aromatic molecules has been relatively few and generally limited to single-ring systems. The relatively weak vibrational intensities for these systems make them challenging candidates for vibrational measurements. Neither ACA nor AA adsorption on metal surfaces has been previously investigated with surface vibrational spectroscopy. With 26 atoms ($C_{14}H_9NO_2$), the free ACA molecule exhibits 72 fundamental vibration modes. Because AA contains one additional atom, it exhibits three more fundamental vibration modes. A preliminary characterization of these normal modes was obtained with quantum chemistry calculations. Density functional theory calculations of normal mode frequencies for the monomers were carried out at B3PW91/6-

311++G**. The calculation results were then scaled according to the empirically determined formula^{82,93}:

$$\nu_{\text{scaled}}=0.955*\nu_{\text{calculated}} + 25.7 \text{ cm}^{-1} \quad (1)$$

for all modes in the infrared region (800 cm⁻¹ -4000 cm⁻¹) accessible in our RAIRS measurements. This calculation method is proven to provide an effective guidance in previous INA study⁹³. The computational results are listed in Tables 1-2, together with reported values for the molecular solid and our present experimental measurements for monolayer structures on Ag(111) obtained at 135 K and 300 K.

5.3.2 AA adsorption on Ag(111) at 300K

We first report results for the chemically simpler AA system. Fig. 5.6 presents a set of RAIR spectra of low coverage (0.1 – 0.4 ML) of Anthroic Acid (AA) adsorbed on Ag(111) at 300 K. A spectrum of condensed phase AA is also provided at the bottom of this figure for comparison. All spectra are dominated by the sharp feature at 1680 cm⁻¹. At 0.1 ML coverage, four more features can be distinguished from the background: two broad features at 3000 and 2600 cm⁻¹, and two sharper features at 3700 and 843 cm⁻¹, respectively. When coverage increases to 0.2 ML, the 3700 cm⁻¹ feature disappears. Meanwhile, a broad band at 900 cm⁻¹ and four sharp features at 1264, 1292, 1414 and 1428 cm⁻¹ appear at 0.2 ML. At 0.4 ML, the 900 cm⁻¹ broad feature splits into a broad band at 933 cm⁻¹ and a sharper band at 883 cm⁻¹. As the coverage increases, the integrated intensity of modes located at 3000, 2600, 1680, 1428, 1414, 1292, 1266, 933 and 883 cm⁻¹ intensify. The only exception is the 843 cm⁻¹ feature, which remains very weak.

No.	Theoretical	Experimental			Description
	B3PW91/6-311++G** (cm ⁻¹)	Monolayer film 300K(cm ⁻¹)	Monolayer film 135K(cm ⁻¹)	Bulk ACA solid (ref)	
30	857			848	γ(CH)
32	873	878			Ring breathing
40	1021			1021	β(CH)
44	1148	1147		1156	β(CH) +β(OH)
47	1261		1234		β(OH)
48	1267		1247		β(OH)
50	1296			1291	β(OH)
51	1348	1305	1319	1318	ν (CO)
53	1385	1376	1370	1395	β(CH)
55	1433	1431	1431	1422	β(CH)
56	1457			1465	β(CH)
57	1482	1494	1486		β(CH)
58	1529		1518		β(OH)+ ν(C=C)
60	1560	1558			ν(C=C)
61	1612	1589			ν(C=C)
63	1756	1638	1711,1655	1653,1607	ν(C=O)
72	3624		3240	3430,3210	ν(O-H)

Table 5.1 Scaled calculation results of ACA monomer with assignments. The experimental results and condensed phase observations are included.

No.	Theoretical	Experimental		Description
	B3PW91/6-311++G** (cm ⁻¹)	Monolayer film at 300K(cm ⁻¹)	Bulk AA solid (ref)	
30	847	843	856	γ (CH)
33	893	883	894	γ (CH)
34	929	933	925	Breathing mode
49	1261		1233	β (OH)
50	1264	1266	1260	β (OH)+ β (CH)
51	1293	1292	1295	β (CH)
53	1354		1345	β (CH)
57	1439	1414	1430	ν (C=C)
58	1445	1428	1449	ν (C=C)
59	1482		1488	ν (C=C)
65	1745	1678	1680	ν (C=O)
75	3627	3700	3033, 2700	ν (O-H)

Table 5.2 Scaled calculation results of AA monomer with assignments. Experimental results and condensed phase observations are included.

To assign these vibrational features, we refer to the reported condensed phase spectra and the quantum computational results. The weak band at 3700 cm^{-1} , which appears only at the lowest 0.1 ML coverage, corresponds to the free hydroxyl stretch mode (calculated at 3627 cm^{-1}), indicating non-H-bonded monomer exists at this coverage. Both broad bands at 3000 and 2600 cm^{-1} are assigned to the hydroxyl stretch under hydrogen bonding influence. The widths and locations of these two modes are comparable with the condensed phase spectrum. Because the solid consists of tail-to-tail dimers, the existence of these hydrogen-bonded hydroxyl stretch modes (3000 cm^{-1} and 2600 cm^{-1}) reveal the formation of AA dimers on Ag(111) even at the lowest coverages at room temperature. The combined presence of free monomer and tail-to-tail dimers proves that AA do not undergo deprotonation.

Further information concerning the extent of hydrogen bond formation is found in the carbonyl stretching region. The strongest mode in the condensed phase spectra is the carbonyl stretch at 1680 cm^{-1} . As discussed in the introduction, AA molecules form tail-to-tail dimers in the bulk crystal. The feature at 1678 cm^{-1} in the RAIR spectra is hence assigned to the carbonyl stretch of AA dimers. The absence of the free carbonyl stretch, which corresponds to the free hydroxyl stretch described above, reflects its low sensitivity at this coverage.

The weak 843 cm^{-1} peak, an in-phase out-of plane C-H bending mode, appearing at 856 cm^{-1} in the condensed phase spectrum, is the only fused-ring mode observable at 0.1 ML coverage. This mode possesses a transition dipole moment perpendicular to the fused-ring plane. The appearance of this feature indicates that at this coverage, 2-D gas AA adsorbs on surface in a predominantly flat-lying geometry.

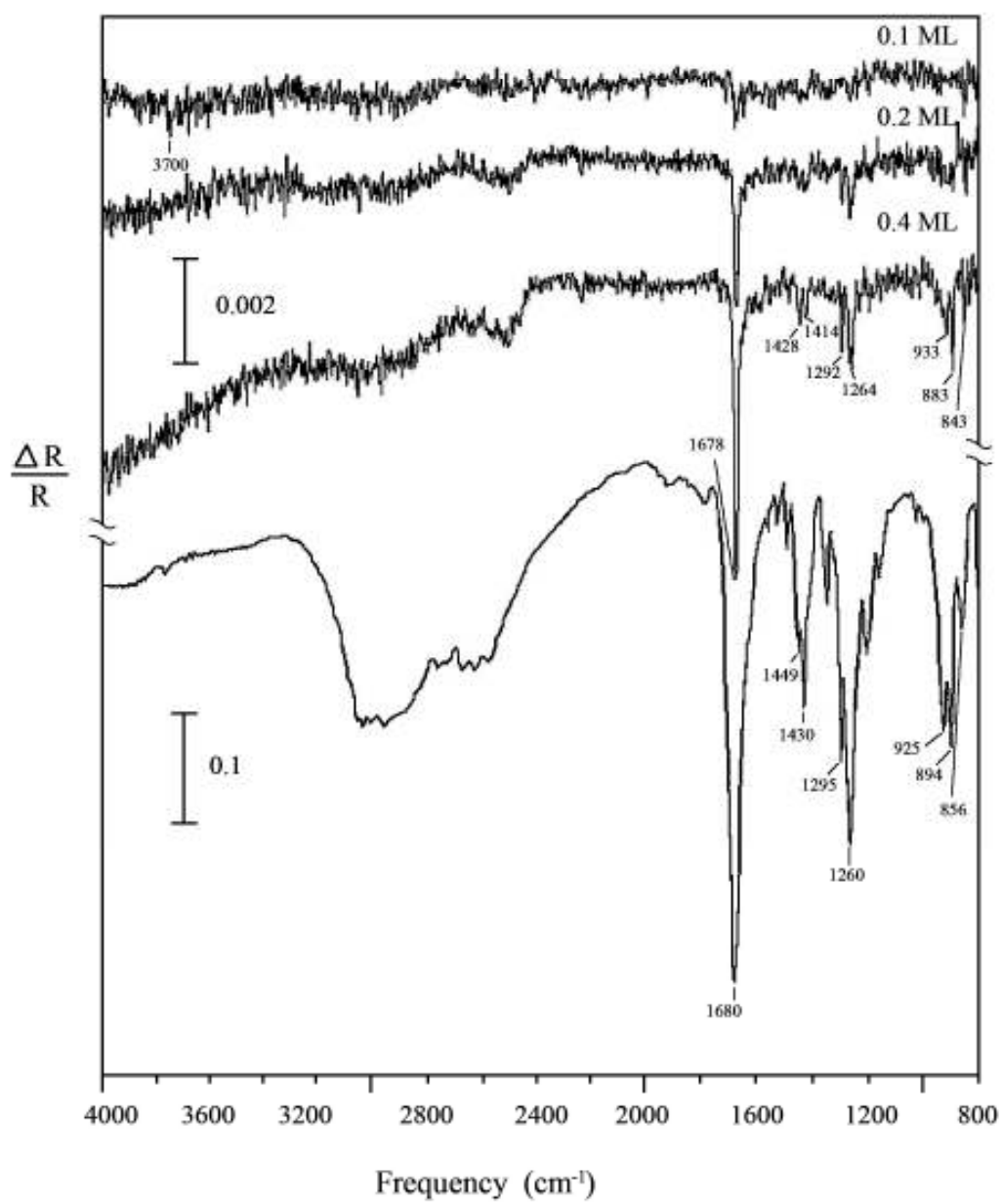


Fig. 5.6 RAIR spectra of AA assembly on Ag(111) at room temperature.

As the exposure increases to higher coverage (0.2 to 0.4 ML), the free hydroxyl stretch mode disappears, indicating that AA monomers only exist at relatively low coverage. Furthermore, the saturation of the out-of-plane C-H bending mode (843 cm^{-1}) signals a change in orientation. This orientation change is further reflected in the emerging spectral features. The 1428 and 1414 cm^{-1} modes correspond to the C=C stretch. The peaks at 1292 and 1264 cm^{-1} are assigned to O-H bending modes coupled with C-H bending. The broad feature at 933 cm^{-1} is a ring breathing mode, and the sharp feature at 883 cm^{-1} is C-H out-of-plane bending mode. At this coverage range, the presence of these C=C stretch modes, which possess transition dipole moments parallel to the ring plane, strongly suggests an inclined orientation. The transition dipole moment of the 1428 cm^{-1} mode is parallel to the ring plane and that of the 883 cm^{-1} mode is predominantly perpendicular to the ring plane (see Fig. 5.6). Thus, these two modes provide a clean set to analyze the ring orientation relative to the surface plane. All the other modes are heavily coupled with the carboxyl vibration and are not suitable to determine the ring orientation unambiguously. The integrated intensity ratio of the 1428 cm^{-1} vs. 883 cm^{-1} bands suggests that the fused-ring is oriented on the surface with a twist angle of $50^\circ \pm 15^\circ$ ⁹³. This relatively large twist angle is completely consistent with the STM images, in which, the packing density of the structures indicates a substantial incline angle. Further evidence is found in X-ray diffraction studies, which reveal that inside each carboxyl-carboxyl dimer, an AA molecule tends to twist relative to its partner to minimize the electrostatic interactions.

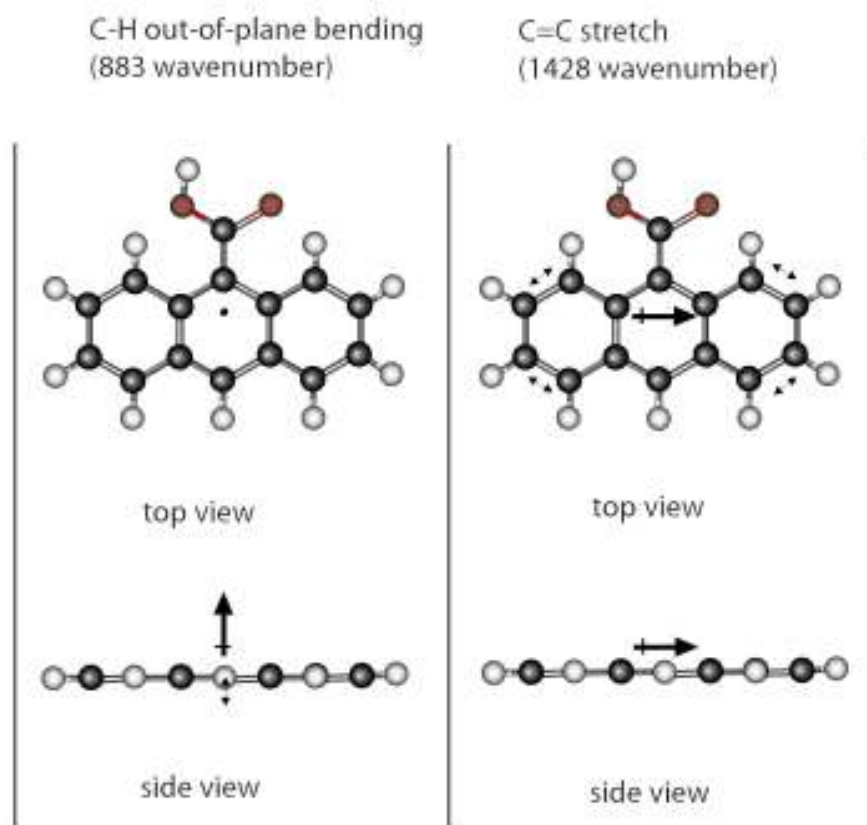


Fig. 5.7 Schematic illustration of C-H out-of-plane bending and C=C stretch modes. The transition dipole moments are illustrated as bold arrows.

Previous studies prove that when heterocyclic molecules adsorb on metal surfaces, the orientation of the adsorbate presents the balance of π -substrate bonding and σ -substrate bonding. As coverage increases, the ring plane tilts up from the surface to enhance the interaction between the lone pair electrons and the substrate. Without the ring nitrogen, AA is incapable of forming σ -bonds to the surface. Hence, the high packing density of AA adlayer structures is mainly due to the fused-ring twisting.

5.3.3 ACA adsorption on Ag(111) at 130 K

We now turn to the vibrational spectra for the ACA heterocycle. To access and explore the varied H-bonding motifs for this system, we have undertaken more comprehensive temperature and coverage dependent measurements. The series of RAIR spectra in Fig. 5.8 represent the initial growth of 9-acridine carboxylic acid (ACA) on Ag(111) at 135K. At low coverage, there are three broad bands: 3244 cm^{-1} (FWHM=120 cm^{-1}), 1709 cm^{-1} (FWHM=40 cm^{-1}) and 1655 cm^{-1} (FWHM=90 cm^{-1}). All three modes intensify as the coverage increases.

The very broad 3244 cm^{-1} band is assigned to the O-H stretch. The location of this mode is close to the O-H stretching mode of condensed ACA, which is 400 cm^{-1} lower than the calculational results for the ACA monomer. The broadness of this mode is typical for hydrogen-bonded O-H stretches. The existence of this mode also immediately rules out a deprotonated adsorption, which is in agreement with our observations from STM and XPS. Thus, the infrared vibrational spectra demonstrate molecular adsorption at low temperatures.

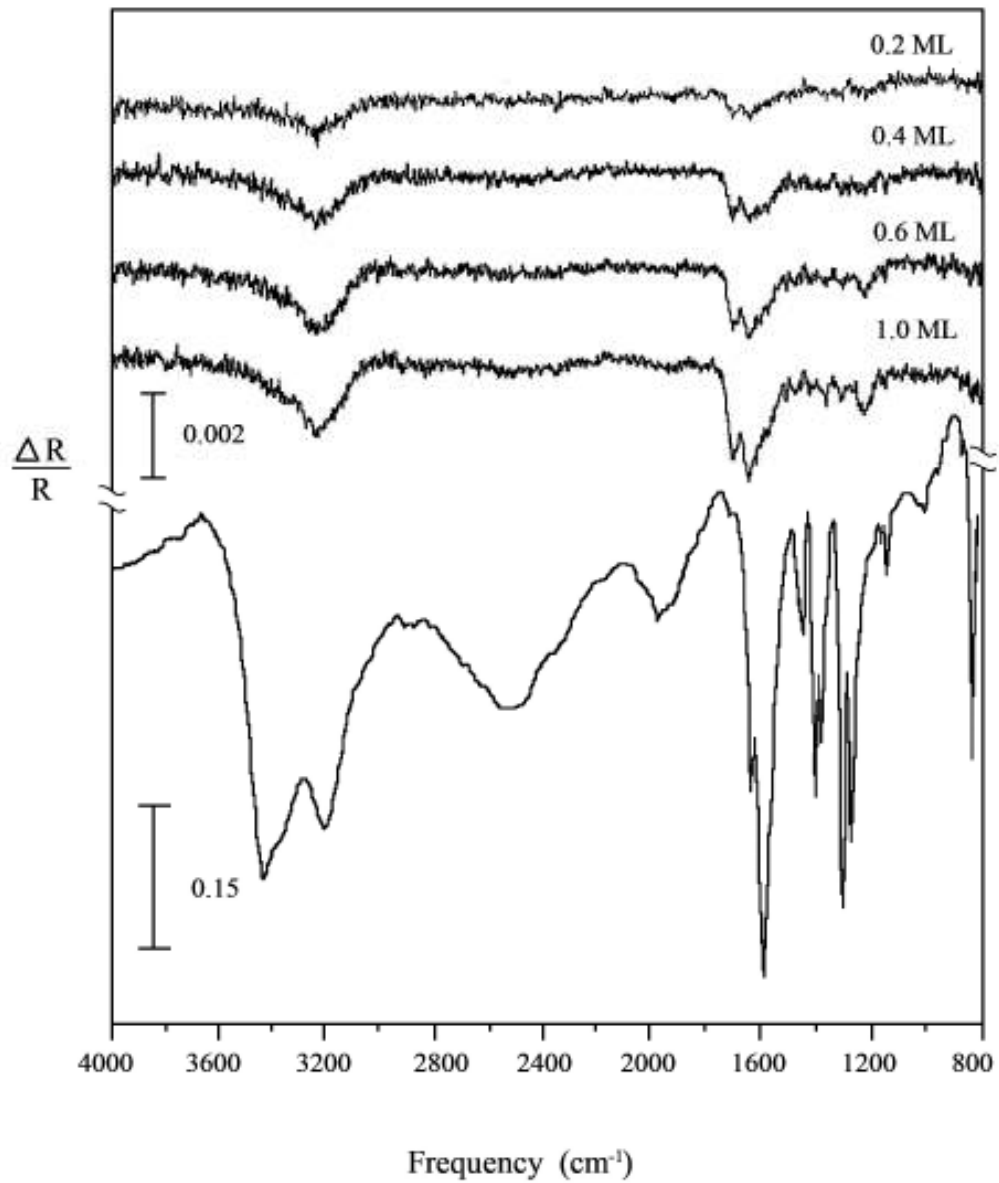


Fig. 5.8 A set of coverage dependent RAIR spectra of ACA adsorption on Ag(111) at 135K. The bottom trace is a reference spectrum of ACA in condensed phase.

Two modes are observed in the carbonyl stretch region: 1709 and 1655 cm^{-1} . Similar doublets are observed in the condensed phase spectrum. However, the frequency and width are quite different. In the condensed phase spectrum, the intense broad feature at 1607 cm^{-1} is assigned to the carbonyl stretch in extensively head-to-tail H-bond chains, while the weak sharp 1653 cm^{-1} feature is attributed to chain fractions and tail-to-tail dimers. Hence, the 1655 cm^{-1} peak in the RAIR spectrum is assigned to the hydrogen-bonded assemblies.

The 1709 cm^{-1} mode represents isolated ACA molecules. At 135 K, ACA will have reduced mobility on the surface, preventing it from organizing into the adlayer structures observed in room temperature STM images. At the lowest coverages the relative intensities of the 1709 cm^{-1} and 1655 cm^{-1} modes indicate that the amount of free ACA and H-bonded ACA are comparable. However, after the coverage exceeds 0.2 ML, the 1655 cm^{-1} feature outgrows the 1709 cm^{-1} feature, indicating that more ACA molecules are involved in hydrogen bond formation. This corroborates with the diffusion limited aggregation of ACA into hydrogen bonded assemblies. With higher coverage, less mobility is required for aggregation.

The shape of the 1655 cm^{-1} vibrational band provides further information about the nature of the hydrogen bonding assembly. The low-frequency tail for the 1655 cm^{-1} mode results from the “cooperative effect”, which is commonly observed in hydrogen-bonded conjugate systems. Such a cooperative effect gradually increases with the growth of hydrogen-bonded chains. The presence of the low-frequency tail provides evidence for the head-to-tail motif. However, the broadness of this feature

indicates that at this coverage and temperature, the surface aggregates are a complex mixture including tail-to-tail dimers and variable length head-to-tail ACA chains.

In principle, the relative intensities of the infrared vibrational bands can also report on the orientation of the ACA molecules. Unlike the single-ringed isonicotinic acid, ACA is a nonplanar molecule. Consequently, the carboxylic acid modes must report on the orientation of the carboxylic acid group, whereas the vibrations associated with the fused rings are needed for a report on the orientation of the aromatic rings. The three ACA modes discussed above (3244 , 1709 and 1655 cm^{-1}) originate with the carboxylic group. The strong intensities of these modes clearly indicate that the carboxylic group is not parallel to the metal surface.

At higher ($0.4 - 1.0\text{ ML}$) coverages, the fingerprint ($1000 - 1600\text{ cm}^{-1}$) region reveals a number of additional vibrational features at 1234 , 1247 , 1319 , 1370 , 1431 , 1486 and 1518 cm^{-1} . The 1234 and 1247 cm^{-1} modes are easily assigned to C-O-H bending motions, further confirming the out-of-plane orientation of the carboxylic group. All other fingerprint modes are assigned to in-plane ring vibrations, signifying that the aromatic rings are appreciably inclined. Ideally, the relative intensities of the in-plane to out-of-plane aromatic ring modes could provide the ring orientation. Unfortunately, all out-of-plane modes fell below 800 cm^{-1} , where our instrumental sensitivity is greatly reduced. Although sensitivity for these very low frequency vibrations precludes quantitative analyses, qualitative conclusions can be drawn from their mere observation. Appearance of in-plane aromatic modes on Ag(111) indicates that the aromatic plane is significantly inclined with respect to the Ag(111) plane. These in-plane modes can be divided into two distinct categories: those with the

dynamic dipole directed along the long-axis of the ring (1319, 1370, 1431 and 1518 cm^{-1}) and those with the dynamic dipole directed along the short axis (840 and 1486 cm^{-1}). The appearance of both sets of modes shows that the orientation of ACA molecules is a combination of appreciable tilt and apparent twist. In the condensed phase ACA spectrum, the in-plane modes are of comparable intensity to the carbonyl stretch. Based upon the relative strength of the in-plane modes to carbonyl stretch, we conclude that the twist angle must exceed the tilt angle. This suggests a twist angle of $\sim 45^\circ$ and a tilt angle of $\sim 20^\circ$.

5.3.4 Temperature dependent measurements

We now investigate the thermal restructure of a 1.0 ML ACA film upon heating. The RAIR spectra in Fig 5.9a-c were recorded as 1.0 monolayer of ACA molecules on Ag(111) at 135K, then subsequently heated to 200 K and 300 K.

The most pronounced spectral changes occur in the carbonyl region. The 135 K carbonyl region consists of components at 1709 cm^{-1} (free carbonyl) and 1655 cm^{-1} (H-bonded carbonyl). As the temperature increases, the intensity of the 1709 cm^{-1} (free carbonyl) band decreases and virtually disappears at 300 K. Simultaneously, the 1655 cm^{-1} band shifts in frequency to 1638 cm^{-1} and increases in integrated intensity. The overall integrated intensity of the carbonyl stretch increases slightly. The increasing intensity proves that the ACA monomers do not desorb from the surface below 300 K, but diffuse on the surface and joint into surface assemblies.

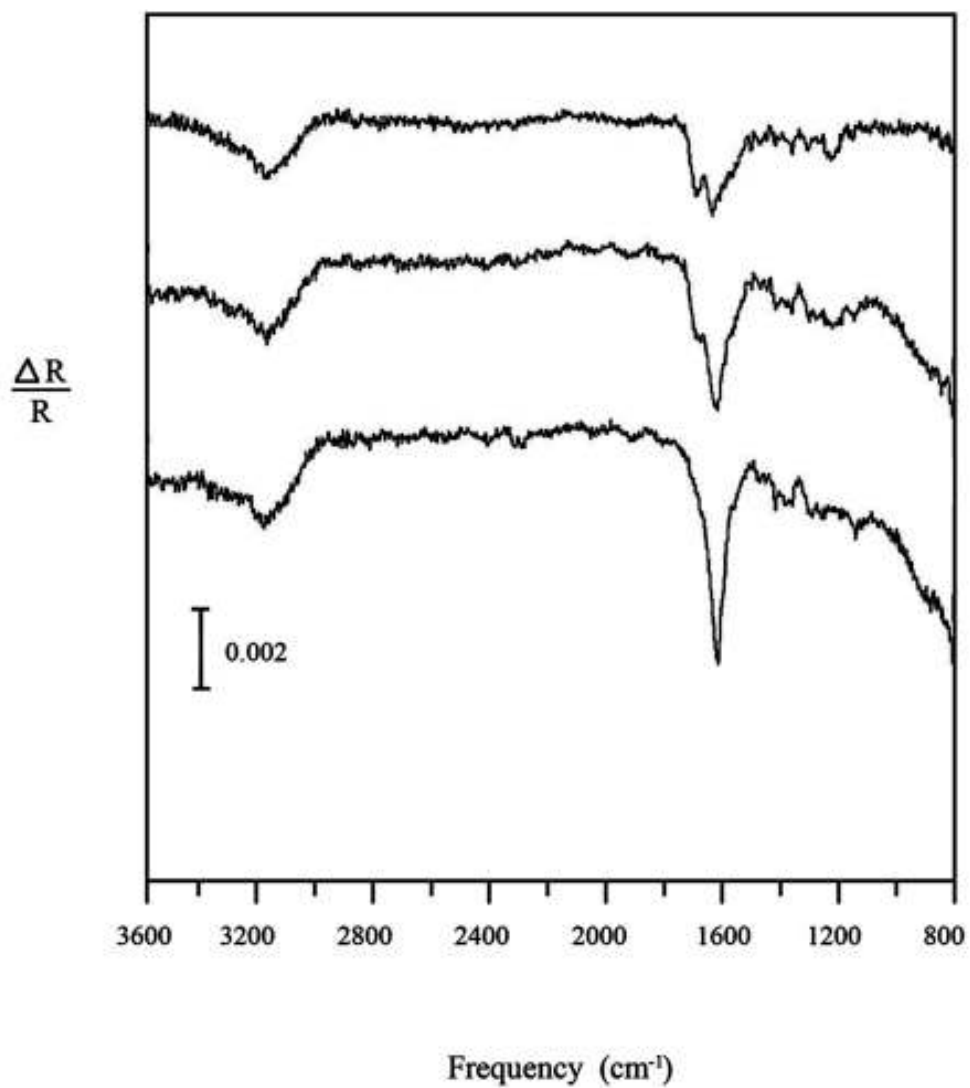


Fig. 5.9 A set of temperature dependent RAIR spectra of 1 ML of ACA films on Ag(111). From top to bottom, the corresponding temperatures are: 135 K, 200 K and 300 K.

The red-shift of the hydrogen bonded carbonyl feature indicates a stronger cooperative effect, which corresponds to longer head-to-tail chains. Therefore, head-to-tail hydrogen bonded chains are proved to be the thermodynamically more stable structure than tail-to-tail hydrogen bonded dimers. This is completely consistent with the room temperature STM observation of the ACA chain phase. The FWHM of this mode remains at 80 cm^{-1} , suggesting that the size of ACA domains stays relatively small, indicating the very slow coarsening of these ACA aggregates at room temperature. The carbonyl feature has ca. 80 cm^{-1} width that is significantly larger than the 16 cm^{-1} width observed for AA. This width increases because there are two inequivalent ACA per unit cell within the chain structure. Moreover, the mode is broadened by the extended H-bonded arrangement.

5.3.5 ACA adsorption on Ag(111) at 300 K

Finally, we turn to ACA adsorption at 300 K, conditions that directly match the previous STM experiments. The RAIR spectra in Fig. 5.10 show the growth of ACA adsorbed on Ag(111) at room temperature. At low coverage (0.2 ML), the only band that can be observed is located at 1638 cm^{-1} (FWHM 65 cm^{-1}). The frequency of the 1638 cm^{-1} band indicates a head-to-tail H-bonded network, which is completely consistent with the STM and XPS results.

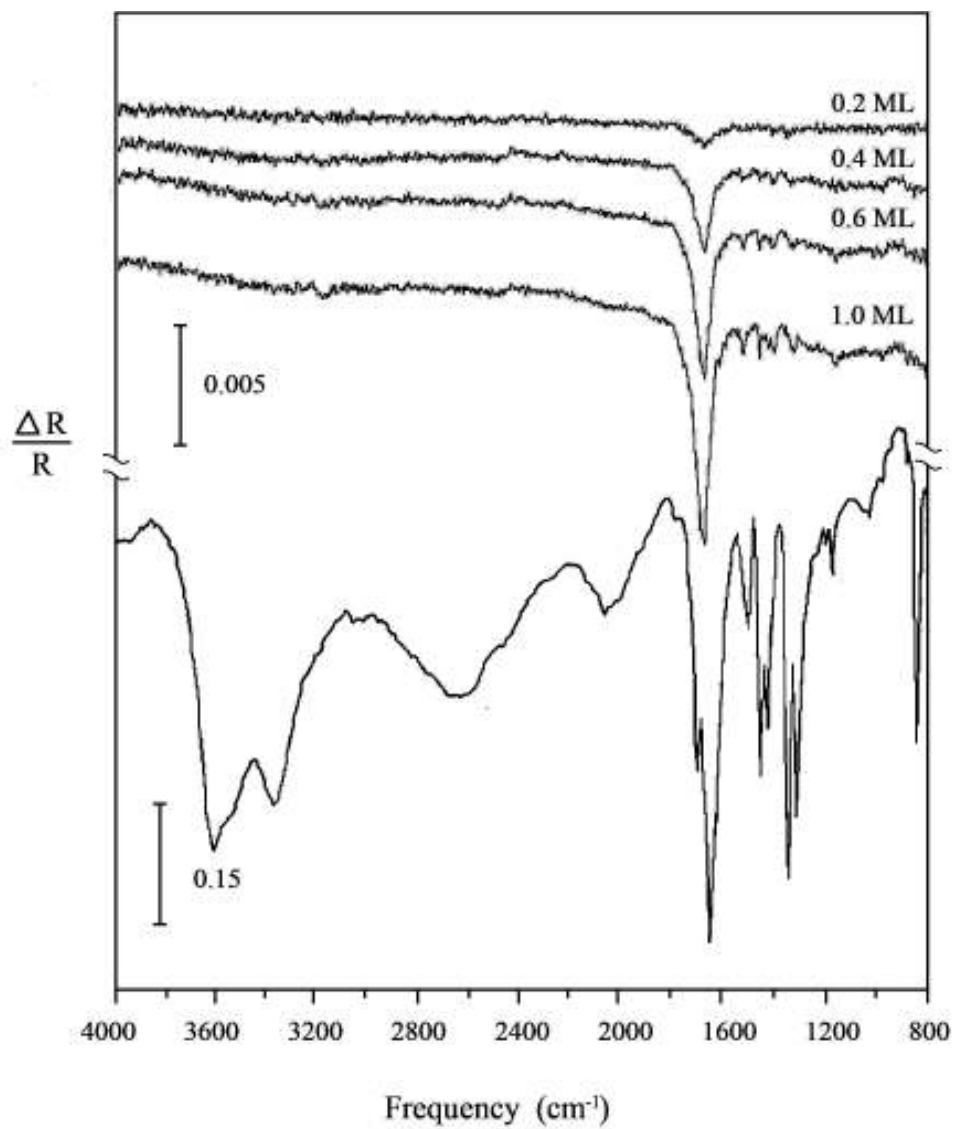


Fig. 5.10 A set of coverage dependent RAIR spectra of ACA adsorption on Ag(111) at room temperature. The bottom trace is a reference spectrum of ACA in condensed phase.

As the coverage increases to 0.4 ML, weak features emerge at 1148, 1304, 1378, 1398, 1433, 1495 and 3200 cm^{-1} . The weak and broad feature at 3200 cm^{-1} is the hydroxyl stretch. The 1304 cm^{-1} band is contributed to the C-O stretch. All of the other modes are assigned to in-plane ring vibration modes. The relative strength of in-plane modes to the carbonyl stretch is higher than observed on the cold substrate. The stronger bands of the in-plane ring features indicate that the incline angle of the molecular ring increases when the temperature is raised from 135 K to 300 K. This incline angle is related to the adlayer architecture. This is consistent with the greater organization into head-to-tail domains at higher temperature.

STM measurements showed a coverage dependent phase transition at room temperature. For coverage lower than 0.4 ML, the surface is covered by the two-dimensional gas phase. Upon coverage increased to 0.4 ML, the head-to-tail chain phase emerges. However, the carbonyl stretch mode (1638 cm^{-1}) does not change frequency while the coverage increases from 0.1 ML to 1.0 ML. The frequency of this mode indicates that in the gas phase, the mobile species on the substrate are not ACA monomers but ACA head-to-tail chains. O'Shea et al. showed that the core level shift of N 1s in INA trimer is similar to the surface core level shift of N 1s in INA thick films³³. Hence, we expect that short head-to-tail chains consisting of 3 to 4 ACA molecules dominate the 2-D gas phase.

Unlike previous STM measurements, we were unable to generate the second ordered phase (dimer phase) on Ag(111) at room temperature. We suspect that this reflects the different measurement time scales in the experiments. In the RAIRS experiments, we are required to collect spectra within one hour of film preparation.

The dimer structures form slowly and their presence is not sufficiently abundant for detection in the IR time window.

A particularly interesting aspect of these room temperature spectra is the relative “silence” of the 1234 and 1247 cm^{-1} bands (C-O-H bending modes), which are observed in contrast to the cryogenic results. There can be two underlying causes. The first is the possible deprotonation of the carboxylic acid. We can rule out deprotonation on the basis of XPS studies on this system at room temperature³⁵. The second possible cause is the orientation of the carboxylic acid group. The absence of all the non-carbonyl carboxylic acid modes indicates that the COH plane is pseudo-parallel to the surface and the carbonyl group is inclined with respect to the surface. Assuming a dihedral angle between the plane of the carboxyl group and the ring plane of 78.9° as observed in the bulk crystal, the fused-ring plane must twist with respect to the surface to achieve this orientation, as shown in Fig. 5.11. The STM derived model of ACA chain phase architecture is based upon a tilt-twist combination orientation. Such a structure is consistent with ACA carboxylic modes intensities.

5.4 Conclusions

Surface assembly of 9-anthroic acid (AA) and 9-acridine carboxylic acid (ACA) on Ag(111) has been investigated using reflection absorption infrared spectroscopy (RAIRS). AA adsorbs on the surface molecularly. At room temperature, AA monomers exist only at very low coverage. Remarkably, the formation of tail-to-tail dimers occurs even in the low coverage range (< 0.1 ML), which STM indicates should be occupied by two-dimensional gas. Further adsorptions reveal that the tail-

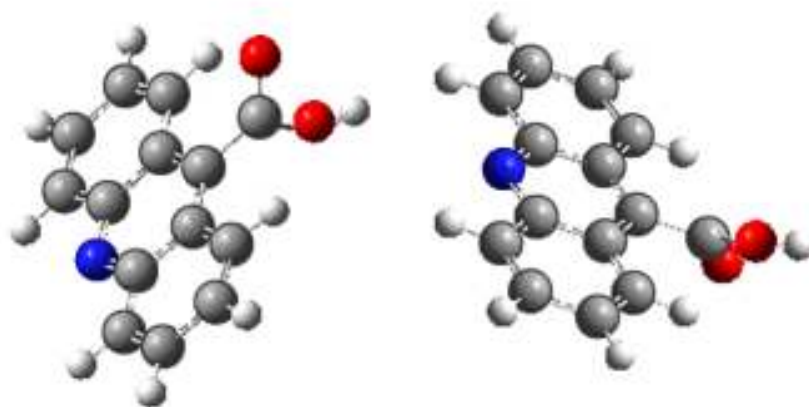


Fig. 5.11 Schematic illustrations of ACA chain structure, based upon fixed 78.1° dihedral angle. Model depicts two inequivalent ACA per unit cell, as observed in STM images, in tilt and twist orientation. Tilt and twist angle of $\sim 50^\circ$ and 45° , respectively, are shown in the figure.

to-tail dimer is the basic building block for all the surface structures. Quantitative analyses of the relative strength of presenting modes indicate that AA molecules adsorbed on the surface with a twist orientation (ca. 50°).

Similar to AA, ACA adsorbed on both cold and room temperature substrates without deprotonation. When adsorption is carried out on cold substrate, a very heterogeneous adlayer structure is formed, in which a diversity of molecular aggregates co-exist with isolated monomers. After annealing to 300 K, a more ordered hydrogen bonded structure is observed. The red shift of the carbonyl stretch mode is completely consistent with an extensive head-to-tail hydrogen bond motif.

The surface assemblies on Ag(111) at room temperature are also stabilized by the formation of head-to-tail hydrogen bonds. Even in two-dimensional gas phase (coverage < 0.4 ML), ACA exist on the surface in the form of head-to-tail H-bonded chains. Unfortunately, the dimer phase (above 1.0 ML) is not observed in RAIRS.

To achieve a thermodynamically stable structure, the molecules take on a tilt-twist orientation to increase the electrostatic interaction among the molecules and the packing density on the surface. This orientation is confirmed by the absence of characteristic features of the hydroxyl group. Constraining the dihedral angle of 78.1° , a tilt angle of 50° and a twist angle of 45° is suggested.

Chapter 6

Thesis Conclusion

In this thesis, I have investigated the adsorption and growth of isonicotinic acid (INA), 9-anthroic acid (AA), and 9-acridine carboxylic acid (ACA) on Ag(111) surfaces.

The adsorption of INA on Ag(111) was studied by STM, XPS and RAIRS. This relatively small organic molecule adsorbs on Ag(111) without deprotonation and forms robust surface structures, which are stabilized by comprehensive hydrogen bond arrangements. A structure model is proposed to describe the surface architecture. INA molecules form long chains along the $[1\bar{1}2]$ direction by head-to-tail couplings. Weak side-linking hydrogen bonds connect these chain structures into 2-D sheets. The surface structure shows substantial similarities to the bulk crystal structures, which should contribute to the same intermolecular interactions. However, the packing density of the surface aggregates reveals the influence of the substrate. Additionally, at submonolayer coverage, 12 rotational domains are observed. They are caused by the 3-fold substrate symmetry, the adsorbate surface-imposed chirality and the head-to-tail hydrogen-bond directions. Each rotational domain contains one enantiomer.

Reflection adsorption infrared spectroscopy confirmed the chemical identities of INA films. Moreover, the orientations of the layered films are determined. The first monolayer orients pseudo-parallel to the surface with a tilt angle of 10° . The subsequent layers have a greater incline angle (30°) with respect to the surface. This

incline angle is interpreted as a 10° tilt combined with a twist rotation along the molecule's long axis. Based upon the results of STM, XPS and RAIRS, a 3-D structural model of isonicotinic acid adsorption on Ag(111) is proposed.

ACA molecules, with distinct electrostatic properties compared to INA molecules, form different assemblies on Ag(111) surface. With two more aromatic rings, the molecule forms stronger π bonding to the substrate. Thus, ACA molecules present lower surface mobility than INAs. Vibrational spectra show that kinetically favored amorphous ACA films are formed on cold substrate. With elevated temperatures, these kinetically favored structures transition into thermodynamically favored head-to-tail hydrogen bond linked chains. Qualitative analyses of the RAIR spectra indicate that ACA molecules present a combined tilt/twist orientation even at submonolayer regime.

To evaluate the role of ring nitrogen in the deposition and growth of these molecular films, I investigated the adsorption of 9-Anthroic Acid on Ag(111). By replacing the ring nitrogen with a C-H group, 9-Anthroic Acid can only form tail-to-tail hydrogen bonded dimers. The sharp band at 1678 cm^{-1} with an FWHM of only 20 cm^{-1} indicates that the surface structure of AA is chemically homogenous. The strong intermolecular electrostatic interactions cause AA molecules to display a twist orientation upon the surface. There is no obvious indication that there exists a substantial tilt orientation in the coverage range. The strong twist (ca. 50°) and weak tilt can be explained by the electronic properties of the aromatic ring. Previous studies reveal that pyridine undergoes an orientational transition as the coverage increases, and the binding to the substrate varies from π -substrate interaction (flat-lying

geometry) to σ -substrate interaction through the lone-pair electrons of the ring nitrogen (tilted orientation). Without a ring nitrogen on the fused-ring, not only is the formation of the head-to-tail hydrogen bond ruled out, but also the σ -substrate interactions at elevated coverage are ruled out. Hence, a tilted orientation is not observed in this system.

We now examine the correlation between bulk crystal structure and monolayer structure. For the present study of INA on Ag(111), the Ag(111) surface has unit cell parameters that are well matched to these of the molecular crystal. Consequently, the INA monolayer contracted only 0.2% along the side link hydrogen bond direction to register to Ag(111). Thus, the monolayer is essentially a plane of the bulk crystal. However, 12 rotational/reflection domains coexist on the surface. For other substrates with significant different lattice constants, such as Cu(111) and Pt(111), the monolayer structure should be perturbed upon the adsorption and a short range ordered structure may be expected.

To achieve better understanding of the adsorption and growth of thin organic films on metal surfaces, a lot of works need to be done. One interesting question is, by changing the surface chemical environments, can the surface structures be controllably altered? For example, the adsorption of aromatic carboxylic acid upon Ag(111)-O surface or other oxide surfaces should lead to carboxylic acid deprotonation. The carboxylate species should adopt a near-perpendicular orientation, in complete contrast to the present studies.

Depositing organic molecules on constrained areas, such as high step density surfaces can be another interesting project. Previous studies reveal that tail-to-tail

dimers have energetic advantages when the growth of long head-to-tail chains is forbidden. The high packing density of tail-to-tail dimers also help to stabilized the structure. Therefore, selecting a high step density surface can encourage the formation of tail-to-tail couplings. In turn, such molecular surfaces also offer new “chemical surfaces” that may prove useful for the templated growth of heteromolecular films.

Appendix A

Fabrication of Ta-Ta₂O₅ film

Argon ion sputtering is extensively used to clean metal surfaces in UHV studies. However, the exact focus point of the Ar⁺ beam used in the sputtering process is hard to determine. In the past, people used fluorescence discs to observe the Ar⁺ epoxy path. The fluorescence radiation is too weak to observe. Moreover, it cannot provide information on the efficiency of the sputtering process. Another way to guide the sputtering process is measuring the sputtering current. Although this technique provides numerical information on the sputtering efficiency, it has a few intrinsic shortcomings. First, it requires that the sputtering target must be electronically floating. Second, it cannot distinguish the metal sample from its metal sample holder. If the Ar⁺ is bombarding the conducting sample holder, a misleading sputtering current can also be read. Third, the sputtering current is very weak (on the order of a microampere); the reading is easily interfered with by the leaking current in the ground system.

In our study, we employed Ta₂O₅ films on Ta substrates to determine the sputtering geometry and operating parameters. The principle of this technique is very straightforward. In the Ta-Ta₂O₅ system, there are two interfaces: vacuum-oxide interface and oxide-metal interface. As a result of the interference of the reflections from these two interfaces, the displayed colors of these films are very sensitive to the thickness. Hence, if a Ta₂O₅ film is placed in the argon ion beam, the sputtering pattern can be readily detected by the eye. Quantitative measurements of thickness

changes can be made with a simple monochromator⁹⁶. The sputtering rate can then be calculated.

The Ta-Ta₂O₅ film is made by anodizing the Ta film in solution. Before anodization, the Ta sheet is cut into 2 cm X 4 cm pieces and then chemically polished for 1 to 2 sec in a mixture of 5 parts 96% H₂SO₄, 1.5 parts 50% HF, and 2 parts 70% HNO₃ by volume. Anodization is then done in 1% Na₂SO₄ solution at a constant current of 60 mA⁹⁷. It takes about 50 seconds to achieve the preferred film thickness of 430 Å, which corresponds to a deep violet color. During sputtering, the film gradually changes color to deep blue, then gold, and at last loses the interference color while approximately 150 Å are removed.

Appendix B

Physical vapor deposition sources

Organic thin films have attracted increasing interest for their potential applications in a variety of advanced technologies, including nonlinear optics, microelectronics, light emitting devices and solar cells. For these applications, one of the challenges is how to control the growth of organic thin films. There are two techniques which are broadly employed in UHV systems. For high vapor pressure (ca. 1×10^{-6} torr) species, backfilling the UHV chamber through a leak valve is an efficient deposition technique. For low vapor pressure molecules, a Knudsen cell is generally used.

N-heteroaromatic acids we studied have low partial vapor pressure at room temperature. At 300 K, their partial pressures are less than 1×10^{-9} torr. A simple back filling through the leak valve is not suitable for these molecules. On the other hand, the temperatures which complete vaporization occurs (580 K for INA, 560 K for ACA and 480 K for AA) are close to the chamber baking temperature, which means the UHV system can be easily contaminated during baking with a Knudsen cell inside the UHV chamber. Consequently, the Knudsen cell must be either cooled during system backing or situated in the load lock.

As shown in Fig. B1, the home-build Knudsen cell is assembled on a standard four-pin 2-3/4" conflate flange. This homebuilt cell is mounted in the load lock for convenient change of deposition materials. A quartz crucible is mounted on top of one copper post. The tungsten wires (Alfa, 99.95%, 0.008") wrap crucible and serve to both support and heat the crucible. A type K thermocouple is inserted into the

crucible for temperature sensing. The molecular material are carefully loaded into the quartz crucible and covered by a thin layer of glass wool. Generally, loose filling to a level of 4 mm suffices for our experiments. Before mounting the Knudsen cell on the load lock, the connections are electronically checked. The resistance of the tungsten wire heating element is ca. 1 Ω , and the resistance of the thermocouple is ca. 3 Ω . This difference also distinguishes the thermocouple pins from the heating element after the Knudsen cell is mounted. We made two similar Knudsen cells with slightly different lengths of the tungsten wires. The heating parameter should be adjusted accordingly. The deposition rates were guided by the thickness monitor. The principle of thickness monitor is, the internal vibration frequency of the quartz crystal is only determined by its mass. With the assumption that all three molecules have a density of 1, each change in the quartz vibration frequency of 1 Hz corresponds to one monolayer. The reading of the thickness monitor suggested that the home build Knudsen cell produces a repeatable vapor flux onto the surface.

As mentioned in Chapter 2, an *in situ* deposition source is required for RAIRS measurements. For *in situ* experiments, a commercial near ambient effusion cell (SPECS NATC) is employed. This cell is heated by a circulated heating fluid, and the temperature of this effusion cell can vary from $-50\text{ }^{\circ}\text{C}$ to $300\text{ }^{\circ}\text{C}$, depending on fluid. During baking, the cell must be water-cooled to retain the cell temperature $< 50\text{ }^{\circ}\text{C}$.

The NATC cell consists of a 25 cm long removable crucible. A filling with ~ 5 mm of loose powder inside the crucible is sufficient for the experiments. Before installation, we insert a pair of thermocouple into the crucible through another $2\frac{3}{4}$ inch flange on the UHV system. The thermocouple provides accurate reading of the

organic chemicals. During experiments, we found that the temperature of the source increased at a slow rate and the actual stabilized temperature was at least 10 K lower than the set point on the heating media controller. The evaporation temperatures (100 °C for both INA and AA, 140 °C for ACA, read from the thermocouple) employed on this source are higher than the temperatures used on the homemade Knudsen cell (80 °C for both INA and AA, 100 °C for ACA). This is contributed to the actual distance between the metal sample and the chemical source is 30 cm for SPECS NATC cell, while this distance for the homemade Knudsen cell is only 5 cm.

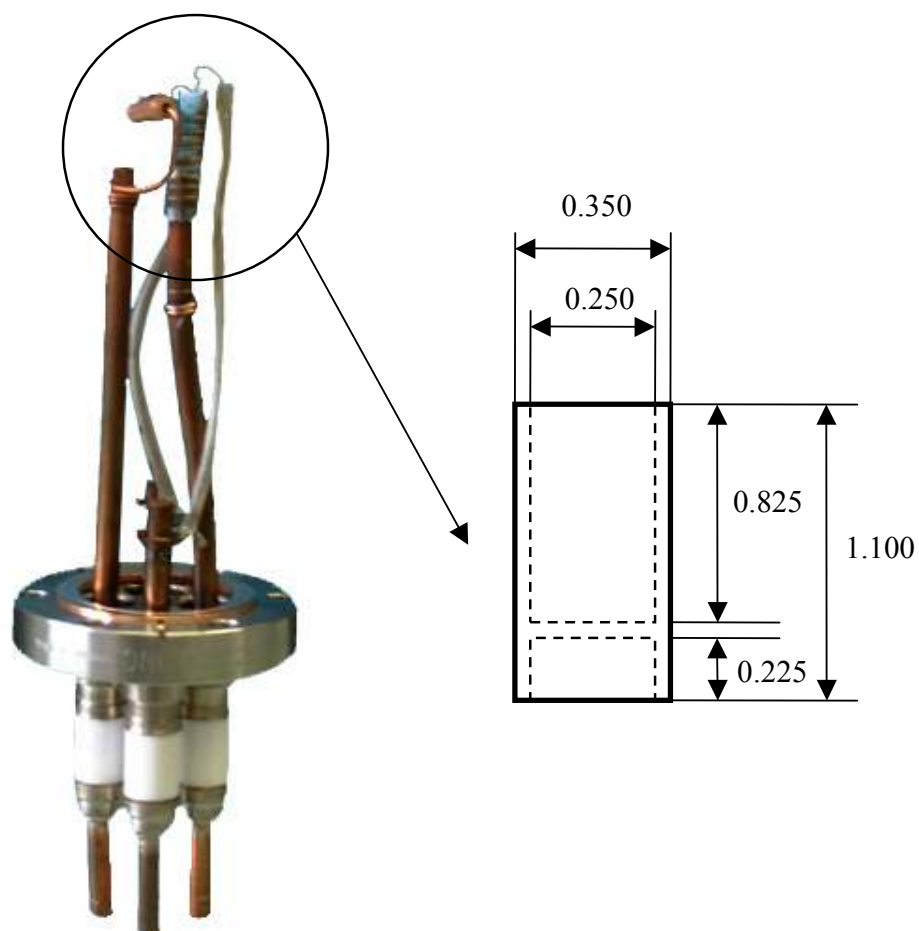


Fig. B1 A picture of the home built Knudsen cell. The dimensions of the quartz crucible are marked. All the numbers are in inches.

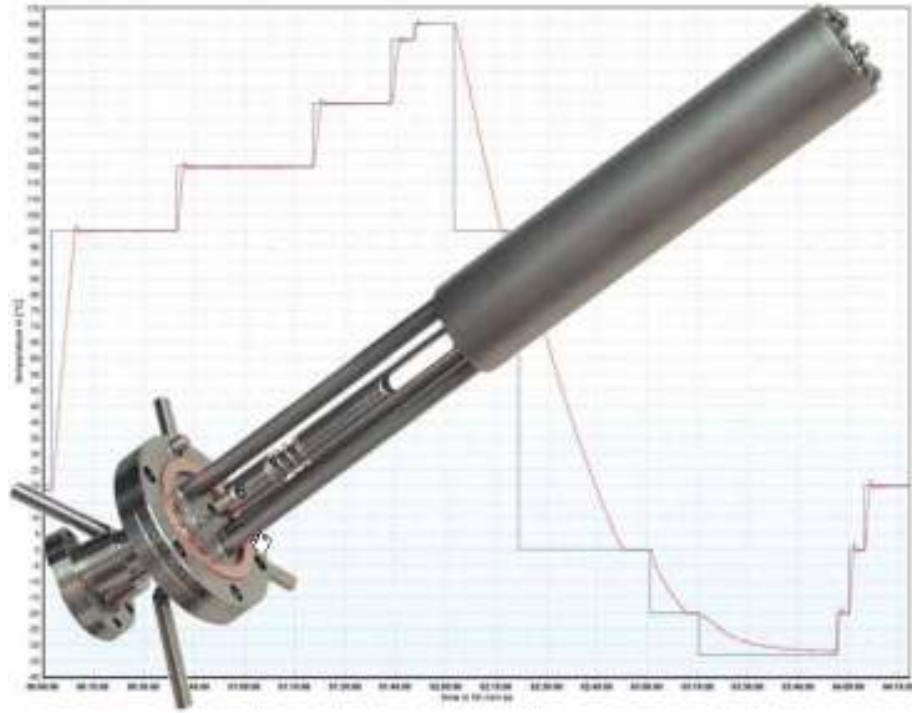


Fig. B2 A photo of Specs NATC cell.

References

1. Ito, T.; Okazaki, S., pushing the limits of lithography. *Nature* **2000**, 406, 1027.
2. C. Joachim; J. K. Gimzewski; Aviram, A., Electronics using hybrid-molecular and mono-molecular devices. *Nature* **2000**, 408, 541.
3. Shirota, Y., organic materials for electronic and optoelectronic devices. *Journal of Materials Chemistry* **2000**, 10, 1.
4. Theobald, J. A.; Oxtoby, N. S.; Phillips, M. A.; Champness, N. R.; Beton, P. H., Controlling molecular deposition and layer structure with supramolecular surface assemblies. *Nature* **2003**, 424, (6952), 1029-1031.
5. Keeling, D. L.; Oxtoby, N. S.; Wilson, C.; Humphry, M. J.; Champness, N. R.; Beton, P. H., Assembly and Processing of Hydrogen Bond Induced Supramolecular Nanostructures. *Nano Lett.* **2003**, 3, (1), 9-12.
6. Barth, J. V.; Weckesser, J.; Cai, C.; Gunter, P.; Burgi, L.; Jeandupeux, O.; Kern, K., Building supramolecular nanostructures at surfaces by hydrogen bonding. *Angew. Chem. Int. Ed.* **2000**, 39, (7), 1230.
7. Böhringer, M.; Morgenstern, K.; Schneider, W.-D.; Berndt, R., Separation of a Racemic Mixture of Two-Dimensional Molecular Clusters by Scanning Tunneling Microscopy. *Angew. Chem. Int. Ed.* **1999**, 38, (6), 821.
8. Stöhr, M.; Wahl, M.; Galka, C. H.; Riehm, T.; Jung, T. A.; Gade, L. H., controlling molecular assembly in two dimensions: The Concentration Dependence of Thermally Induced 2D Aggregation of Molecules on a Metal Surface. *Angew. Chem. Int. Ed.* **2005**, 44, 7394.

9. Berner, S.; Brunner, M.; Ramoino, L.; Suzuki, H.; Guntherodt, H. J.; Jung, T. A., Time evolution analysis of a 2D solid-gas equilibrium: a model system for molecular adsorption and diffusion. *Chemical Physics Letters* **2001**, 348, (3-4), 175-181.
10. Yokoyama, T.; Yokoyama, S.; Kamikado, T.; Okuno, Y.; Mashiko, S., selective assembly on a surface of supramolecular aggregates with controlled size and shape. *Nature* **2001**, 413, 619.
11. Stepanow, S.; Lingenfelder, M.; Dmitriev, A.; Spillmann, H.; Delvigne, E.; Lin, N.; Deng, X.; Cai, C.; Barth, J. V.; Kern, K., Steering molecular organization and host-guest interactions using two-dimensional nanoporous coordination systems. *Nature Materials* **2004**, 3, 229.
12. Dmitriev, A.; Spillmann, H.; Lin, N.; Barth, J. V.; Kern, K., Modular assembly of two-dimensional metal-organic coordination Networks at a metal surface. *Angew. Chem. Int. Ed.* **2003**, 42, 2670.
13. Nuzzo, R. G.; Allara, D. L., adsorption of bifunctional organic disulfides on gold surfaces. *J. Am. Chem. Soc.* **1983**, 105, 4481.
14. Nuzzo, R. G.; Fusco, F. A.; Allara, D. L., spontaneously organized molecular assemblies. *J. Am. Chem. Soc.* **1987**, 109, 2358.
15. Yeganeh, M. S.; Dougal, S. M.; Polizzotti, R. S.; Rabinowitz, P., interfacial atomic structure of a self-assembled alkyl thiol monolayer/Au(111): a sum-frequency generation study. *Physical Review Letters* **1995**, 74, 1811.

16. Kafer, D.; Witte, G.; Cyganik, P.; Terfort, A.; Woll, C., a comprehensive study of self-assembled monolayers of anthracenethiol on Gold: solvent effects, structure, and stability. *J. Am. Chem. Soc.* **2006**, 128, 1723.
17. Wuhn, M.; Weckesser, J.; Woll, C., Bonding and Oeientational Ordering of Long-chain carboxylic acids on Cu(111): investigations using X-ray absorption spectroscopy. *Langmuir* **2001**, 17, 7605.
18. Allara, D. L.; Nuzzo, R. G., Spontaneously organized molecular assemblies. 1. Formation, dynamics, and physical properties of n-alkanioc acids on an oxidized aluminum surface. *Langmuir* **1985**, 1, 52.
19. Allara, D. L.; Nuzzo, R. G., Spontaneously organized molecular assemblies. 2. Quantitative infrared spectroscopic determination *Langmuir* **1985**, 1, 52.
20. Ogawa, H.; Chihara, T.; Taya, K., Selective monomethyl esterification of dicarboxylic acids by use of monocarboxylate chemisorption on alumina. *J. Am. Chem. Soc.* **1985**, 107, 1365.
21. Chen, Q.; Perry, C. C.; Frederick, B. G.; Murray, P. W.; Haq, S.; Richardson, N. V., structural aspects of the low-temperature deprotonation of benzoic acid on Cu(110) surfaces. *Surface Science* **2000**, 446, 63.
22. Neuber, M.; Zharnikov, M.; Walz, J.; Grunze, M., The adsorption geometry of benzoic acid on Ni(110). *Surface Review & Letters* **1999**, 6, (1), 53.
23. Demuth, J. E.; Christmann, K.; Sanda, P. N., *Chemical Physics Letters* **1980**, 76, 201.
24. Barth, J. V.; Weckesser, J.; Trimarchi, G.; Vladimirova, M.; Vita, A. D.; Cai, C.; Brune, H.; Gunter, P.; Kern, K., stereochemical effects in supramolecular self-

assembly at surfaces: 1-D versus 2-D enantiomorphic ordering for PVBA and PEBA on Ag(111). *J. Am. Chem. Soc.* **2002**, 124, 7991.

25. J. Weckesser; A. De Vita; J.V. Barth; C. Cai; Kern, K., Mesoscopic correlation of supramolecular chirality in one-dimensional Hydrogen-bonded Assemblies. *Physical Review Letters* **2001**, 87, (9), 096101.

26. Clair, S.; Pons, S.; Seitsonen, A. P.; Brune, H.; Kern, K.; Barth, J. V., STM study of terephthalic acid self-assembly on Au(111): hydrogen-bonded sheets on an inhomogeneous substrate. *J. Phys. Chem. B* **2004**, 108, 14585.

27. Barth, J. V.; Weckesser, J.; Lin, N.; Dmitriev, A.; Kern, K., Supramolecular architectures and nanostructures at metal surfaces. *Applied Physics A: Materials Science & Processing* **2003**, 76, (5), 645-652.

28. Barth, J. V.; Costantini, G.; Kern, K., Engineering atomic and molecular nanostructures at surfaces. *Nature* **2005**, 437, (7059), 671-679.

29. A. Dmitriev; N. Lin; J. Weckesser; J. V. Barth; Kern, K., Supramolecular Assemblies of Trimesic Acid on a Cu(100) Surface. *J. Phys. Chem. B* **2002**, 106, 6907.

30. Suzuki, S.; Green, P. G.; Bumgarner, R. E.; Dasgupta, S.; Goddard, W. A. I.; Blake, G. A., benzene forms hydrogen bonds with water. *Science* **1992**, 257, 942.

31. Mdluli K; Slayden RA; Zhu Y; Ramaswamy S; Pan X; Mead D; Crane DD; Musser JM; 3rd., B. C., Inhibition of a Mycobacterium tuberculosis beta-ketoacyl ACP synthase by isoniazid. *Science* **1998**, 280, 1607.

32. Stephen M. Downs; Joshua Cottom; Hunzicker-Dunn, M., Protein kinase C and meiotic regulation in isolated mouse oocytes. *Molecular Reproduction and Development* **2001**, 58, 101.
33. Takusagawa, F.; Shimada, A., Isonicotinic acid. *Acta Crystallographica Section B* **1976**, 32, (6), 1925-1927.
34. James N. O'shea; Joachim Schnadt; Paul A. Bruhwiler; Hendrik Hillesheimer; Nils Martensson; Luc Patthey; Juraj Krempasky; ChuanKui Wang; Yi Luo; Agren, H., Hydrogen-Bond Induced surface core-level shift in isonicotinic acid. *J. Phys. Chem. B* **2001**, 105, (10), 1917.
35. J. Schnadt; J.N. O'Shea; L. Patthey; J. Schiessling; J. Krempasky; M. Shi; N. Martensson; Bruhwiler, P. A., Structural study of adsorption of isonicotinic acid and related molecules on rutile TiO₂(110) II: XPS. *Surface Science* **2003**, 544, 74.
36. Bo Xu; Bindhu Varughese; Diane Evans; Reutt-Robey, J., Morphology Selected Molecular Architecture: Acridine Carboxylic Acid Monolayers on Ag(111). *J. Phys. Chem. B* **2006**, 110, (3), 1271.
37. Xu, B.; Tao, C.; Williams, E. D.; Reutt-Robey, J. E., Coverage Dependent Supramolecular Structures: C₆₀:ACA Monolayers on Ag(111). *J. Am. Chem. Soc.* **2006**, 128, (26), 8493-8499.
38. Parker, B.; Immaraporn, B.; Gellman, A. J., carboxylic acid deprotonation on the Ag(110) and Ag(111) surfaces. *Langmuir* **2001**, 17, 6638.
39. Spillmann, H.; Dmitriev, A.; Lin, N.; Messina, P.; Barth, j. V.; Kern, K., Hierarchical assembly of two-dimensional homochiral nanocavity arrays. *journal of the american chemical society* **2003**, 125, 10725.

40. Wei, Y.; Kannappan, K.; Flynn, G. W.; Zimmt, M. B., Scanning Tunneling Microscopy of Prochiral Anthracene Derivatives on Graphite: Chain Length Effects on Monolayer Morphology. *Journal of the American Chemical Society* **2004**, 126, 5318.
41. Schnadt, J.; O'shea, J. N.; Patthey, L.; Schiessling, J.; Krempasky, J.; Shi, M.; Martensson, N.; Bruhwiler, P. A., Structural study of adsorption of isonicotinic acid and related molecules on rutile TiO₂(1 1 0) II: XPS. *Surface Science* **2003**, 544, (1), 74-86.
42. Bitzer, T.; Richardson, N. V.; Reiss, S.; Wuhn, M.; Woll, C., sodium-induced ordering of the benzoate species on Si(100)-2x1: a combined HREELS, XPS and NEXAFS study. *Surface Science* **2000**, 458, 173.
43. L. Patrone; S. Palacin; J. Charlier; F. Armand; J. P. Bourgoin; Tang, H.; Gauthier, S., Evidence of the key role of metal-molecule bonding in metal-molecule-metal transport experiments. *Physical Review Letters* **2003**, 91, 096802.
44. W. Wei; W.X. Huang; J.M.White, Adsorption of styrene on Ag(111). *Surface Science* **2004**, 572, 401-408.
45. Eremtchenko, M.; bauer, D.; schaefer, J. A.; Tautz, F. S., Polycyclic aromates on close-packed metal surfaces: functionalization, molecular chemisorption and organic epitaxy. *New Journal of Physics* **2004**, 6, 4.
46. Allegretti, F.; Renzi, V. D.; Biagi, R.; Pennino, U. d.; Contini, G.; Castro, V. D.; Mariani, C.; Betti, M. G.; Fontanesi, C., HREELS study of the adsorption mechanism and orientational order of 2-mercaptobenzoxazole on Cu(100). *surface science* **2003**, 539 63.

47. A.R. Garcia; J.L. da Silva; Ilharco, L. M., chemical adsorption of acetic acid and deuterated acetic acid on Ru(0001), by RAIRS. *Surf. Sci.* **1998**, 415, 183.
48. Yamada, T.; Shirasaka, K.; Takano, A.; Kawai, M., adsorption of cytosine, thymine, guanine and adenine on Cu(10) studied by infrared reflection absorption spectroscopy. *Surface Science* **2004**, 561, 233.
49. Zangwill, A., *Physics at Surfaces* Cambridge University Press, Cambridge: 1988.
50. Smith, B. C., *Fundamentals of Fourier Transform Infrared Spectroscopy*. CRC Press, Inc.: Boca Raton, 1996.
51. Go, E. Hydrogen adsorption and mass flow on vicinal Al(111) surfaces: combined STM-Infrared study. University of Maryland, College Park, 1999.
52. Baski, A. A.; Fuchs, H., Epitaxial growth of silver on mica as studied by AFM and STM. *Surface Science* **1994**, 313, (3), 275-288.
53. F. S. Tautz; M. Eremitchenko; J. A. Schaefer; M. Sokolowski; V. Shklover; K. Glocker; Umbach, E., a comparison of the chemisorption behaviour of PTCDA on different Ag surfaces. *Surface Science* **2002**, 502-503, 176-184.
54. Weckesser, J.; Vita, A. D.; Barth, J. V.; Cai, C.; Kern, K., mesoscopic correlation of supramolecular chirality in one-dimensional hydrogen-bonded assemblies. *Physical Review Letters* **2001**, 87, 096101-1.
55. Witte, G.; Woll, C., organic surface science: creating order and complexity using self-assembly. *Phase Transitions: a Multinational Journal* **2003**, 76, (4-5), 291.
56. Dmitriev, A.; Lin, N.; Weckesser, J.; Barth, J. V.; Kern, K., supramolecular assemblies of trimesic acid on a Cu(100) surface. *J. Phys. Chem. B* **2002**, 106, 6907.

57. Kamat, J. P.; Devasagayam, T. P. A., nicotinamide (vitamin B3) as an effective antioxidant against oxidative damage in rat brain mitochondria. *Redox Report* **1999**, 4, (4), 179.
58. Johnsson, K.; King, D. S.; Schultz, P. G., studies on the mechanism of action of isoniazid and ethionamide in the chemotherapy of tuberculosis. *Journal of the American Chemical Society* **1995**, 117, (17), 5009.
59. O'Regan, B.; Gratzel, M., a low-cost, high-efficiency solar cell based on dye-sensitized colloidal tio₂ films. *Nature* **1991**, 353, 737.
60. Evans, D.; Reutt-Robey, J. E., **Unpublished Data**.
61. Tao, F.; Goswami, J.; Bernasek, S. L., *Journal of Physical Chemistry B* **2006**, 110, 4199.
62. Xu, B.; Tao, C.; Cullen, W.; Reutt-Robey, J.; Willams, E., Chiral symmetry breaking in two-dimensional C₆₀-ACA intermixed systems. *Nano Letters* **2005**, 5, (11), 2207.
63. Horowitz, G., organic thin film transistors: from theory to real devices. *Journal of Materials Research* **2004**, 19, (7), 1946.
64. Tal, O.; Rosenwaks, Y.; Preezant, Y.; Tessler, N.; Chan, C. K.; Kahn, A., Direct Determination of the Hole Density of States in Undoped and Doped Amorphous Organic Films with High Lateral Resolution. *Physical Review Letters* **2005**, 95, (25), 256405.
65. Peumans, P.; Uchida, S.; Forrest, S. R., Efficient bulk heterojunction photovoltaic cells using small-molecular-weight organic thin films. *Nature* **2003**, 425, 158.

66. Tang, C. W., Two-layer organic photovoltaic cell. *Applied Physics Letters* **1986**, 48, 183.
67. Pribat, D.; Plais, F., Matrix addressing for organic electroluminescent displays. *Thin Solid Films* **2001**, 383, 25.
68. Pfeiffer, M.; Leo, K.; Zhou, X.; Huang, J. S.; Hofmann, M.; Werner, A.; Blochwitz-Nimoth, J., Doped organic semiconductors: physics and application in light emitting diodes. *Organic Electronics* **2003**, 4, 89.
69. Li, H.; Xu, B.; Evans, D.; Reutt-Robey, J. E., Isonicotinic acid molecular films on Ag(111): I. XPS and STM studies of orientational domains. **to be published**.
70. Chabal, Y. J., surface infrared spectroscopy. *Surf. Sci. Rep.* **1988**, 8, 214.
71. Jingfu Fan; Trenary, M., symmetry and the surface infrared selection rule for the determination of the structure of molecules on metal surfaces. *Langmuir* **1994**, 10, 3649.
72. Hostetler, M. J.; Manner, W. L.; Nuzzo, R. G.; Girolami, G. S., Two-dimensional melting transitions of rod-like molecules analyzed by reflection-absorption infrared spectroscopy. *Journal of Physical Chemistry* **1995**, 99, 15269.
73. Vincent Humblot; Maria Ortega Lorenzo; Christopher J. Baddeley; Sam Haq; Raval, R., Local and Global Chirality at Surfaces: Succinic Acid versus Tartaric Acid on Cu(110). *J. Am. Chem. Soc.* **2004**, 126, 6460.
74. Sim, W. S.; Gardner, P.; King, D. A., Surface-Bound Helical Polyacetaldehyde Chains and Bidentate Acetate Intermediates on Ag{111}. *J. Am. Chem. Soc.* **1996**, 118, (41), 9953-9959.

75. McNutt, A.; Haq, S.; Raval, R., RAIRS investigations on the orientation and intermolecular interactions of adenine on Cu(110). *Surface Science* **2003**, 531, 131.
76. Nuzzo, R. G.; Dubois, L. H.; Allara, D. L., Fundamental studies of microscopic wetting on organic surfaces. 1. Formation and structural *J. Am. Chem. Soc.* **1990**, 112, 558.
77. Ralph, G. N.; Eileen, M. K.; Lawrence, H. D., Studies of the temperature-dependent phase behavior of long chain n-alkyl thiol monolayers on gold. *The Journal of Chemical Physics* **1990**, 93, (1), 767-773.
78. Nicholas, C., III; Christopher, E. D. C.; Gang-yu, L.; Giacinto, S., Superlattice structure at the surface of a monolayer of octadecanethiol self-assembled on Au(111). *The Journal of Chemical Physics* **1993**, 98, (4), 3503-3511.
79. Fenter, P.; Eberhardt, A.; Eisenberger, P., self-assembly of n-alkyl thiols as disulfides on Au(111). *Science* **1994**, 266, 1216.
80. Fenter, P.; Eisenberger, P.; Liang, K. S., Chain-length dependence of the structures and phases of $\text{CH}_3(\text{CH}_2)_{n-1}\text{SH}$ self-assembled on Au(111). *Physical Review Letters* **1993**, 70, (16), 2447.
81. Frisch, M. J.; Trucks, G. W.; Schlegel, H. B.; Scuseria, G. E.; Robb, M. A.; Cheeseman, J. R.; Zakrzewski, V. G.; Montgomery, J. A.; Stratmann, R. E.; Burant, J. C.; Daapprich, S.; Millaim, J. M.; Daniels, A. D.; Kudin, K. N.; Strain, M. C.; Farkas, O.; Tomasi, J.; Barone, V.; Cossi, M.; Cammi, R.; Mennucci, B.; Pomelli, C.; Adamo, D.; Clifford, S.; Ochterski, J.; Petersson, G. A.; Ayala, P. Y.; Cui, Q.; Morokuma, K.; Malick, D. K.; Rabuck, A. D.; Raghavachari, K.; Foresman, J. B.; Cioslowski, J.; Ortiz, J. V.; Stefanov, B. B.; Liu, G.; Liashenko, A.; Piskorz, P.;

Komaromi, I.; Gomperts, R.; Martin, R. L.; Fox, D. J.; Keith, T. A.; ALLaham, M. A.; Peng, C. Y.; Nanayakkara, A.; Gonzales, C.; Challacombe, M.; Gill, P. M. W.; Johnson, B. G.; Chen, W.; Wong, M. W.; Andres, J. L.; Replogle, E. S.; Head-Gordon, M.; Replogle, E. S.; Pople, J. A., *Gaussian 98 (Revision A.8)*, Gaussian, Inc., Pittsburgh PA, 1998.

82. Palafox, M. A., *International Journal of Quantum Chemistry* **2000**, 77, 661.

83. Rode, J. E.; Dobrowolski, J. C.; Jamroz, M. H.; Borowiak, M. A., theoretical IR, Raman and NMR spectra of 1,2- and 1,3-dimethylenecyclobutane. *Vibrational Spectroscopy* **2001**, 25, 133.

84. P. Koczon; J. Cz. Dobrowolski; W. Lewandowski; Mazurek, A. P., Experimental and theoretical IR and Raman spectra of picolinic, nicotinic and isonicotinic acids. *Journal of Molecular Structure* **2003**, 655, 89-95.

85. Jeffrey, G. A., Hydrogen-bonding: an update. *Crystallography Reviews* **2003**, 9, 135.

86. Zwier, T. S., THE SPECTROSCOPY OF SOLVATION IN HYDROGEN-BONDED AROMATIC CLUSTERS. *Annual Review of Physical Chemistry* **1996**, 47, (1), 205-241.

87. Reed, A. e.; Durtiss, L. A.; Weinhold, F., Intermolecular interactions from a natural bond orbital, donor-acceptor viewpoint. *Chemical Reviews* **1988**, 88, 899.

88. Lee, J. G.; Ahner, J.; Yates, J. T., Adsorption Geometry of 4-Picoline Chemisorbed on the Cu(110) Surface: A Study of Forces Controlling Molecular Self-Assembly. *J. Am. Chem. Soc.* **2002**, 124, (11), 2772-2780.

89. Richardson, N. V., some recent investigations of adsorbate/metal interactions by electro energy loss spectroscopy. *Vacuum* **1983**, 33, 787.
90. Johnson, A., L.; Muetterties, E. L.; Stohr, J.; Sette, F., chemisorption geometry of pyridine on Pt(111) by NEXAFS. *Journal of Physical Chemistry* **1985**, 89, 4071.
91. Gador, D.; Buchberger, C.; Fink, R.; Umbach, E., "Manipulation" of molecular orientation in ultrathin organic films: NTCDA on Ag(111). *Europhysics Letters* **1998**, 41, (2), 231.
92. Yang, M. C.; Rockey, T. J.; Pursell, D.; Dai, H. L., Layer-by-layer structure in ultrathin aniline and pyridine films on Ag(111). *J. Phys. Chem. B* **2001**, 105, 11945.
93. Li, H.; Xu, B.; Evans, D.; Reutt-Robey, J. E., An RAIRS probe of layer-dependent isonicotinic acid architecture on Ag(111). *to be published* **2006**.
94. Patel, N. E.; Reutt-Robey, J. E., *Acta Crystallogr., Sect. E: Struct. Rep.* **submitted for publication**.
95. Xu, B.; Reutt-Robey, J. E., *University of Maryland to be published*.
96. Nielsen, R. E.; Shepherd, W. B., simple technique of examination of sputtering patterns. *Review of Scientific Instruments* **1963**, 35, 123.
97. Vermilyea, D. A., the kinetics of formation and structure of anodic oxide films on tantalum. *Acta Metallurgica* **1953**, 1, 282.